Journal of Biomedical Optics

SPIEDigitalLibrary.org/jbo

Fiber-optic sensors for monitoring patient physiological parameters: a review of applicable technologies and relevance to use during magnetic resonance imaging procedures

Łukasz Dziuda

SPIE

Journal of Biomedical Optics 20(1), 010901 (January 2015)

REVIEW

Fiber-optic sensors for monitoring patient physiological parameters: a review of applicable technologies and relevance to use during magnetic resonance imaging procedures

Łukasz Dziuda*
Military Institute of Aviation Medicine, Technical Department of Aeromedical Research and Flight Simulators, Krasińskiego 54/56, Warszawa, 01-755 Poland

Abstract. The issues involved with recording vital functions in the magnetic resonance imaging (MRI) environment using fiber-optic sensors are considered in this paper. Basic physiological parameters, such as respiration and heart rate, are fundamental for predicting the risk of anxiety, panic, and claustrophobic episodes in patients undergoing MRI examinations. Electronic transducers are generally hazardous to the patient and are prone to erroneous operation in heavily electromagnetically penetrated MRI environments; however, nonmetallic fiber-optic sensors are inherently immune to electromagnetic effects and will be crucial for acquiring the above-mentioned physiological parameters. Forty-seven MRI-tested or potentially MRI-compatible sensors have appeared in the literature over the last 20 years. The author classifies these sensors into several categories and subcategories, depending on the sensing element placement, method of application, and measurand type. The author includes five in-house-designed fiber Bragg grating based sensors and shares experience in acquiring physiological measurements during MRI scans. This paper aims to systematize the knowledge of fiber-optic techniques for recording life functions and to indicate the current directions of development in this area. [DOI: 10.1117/1.JBO.20.1.010901]

Keywords: fiber-optic sensors; claustrophobia; clinical applications; imaging systems; medical monitoring; physiological parameters.

Paper 140519VR received Aug. 15, 2014; accepted for publication Dec. 8, 2014; published online Jan. 16, 2015.

1 Introduction

Continuous monitoring of human physiological parameters throughout a 24-h activity cycle is becoming more common, and new application areas are continually being developed. Devices for recording vital functions have long been used outside of the doctor's office, e.g., athletes use personal recorders to control their training intensity.[1] Moreover, the development of wireless data transmission technologies and teletransmission has resulted in the creation of many home monitoring systems, which are capable of recording and independently transmitting medical parameters to a patient service center.[2] If clinically significant changes are observed in the analyzed data, the supervising doctor is notified by a short message service, e-mail, or fax so that an appropriate treatment can be specified.

Similar systems have been implemented for monitoring drivers, machine operators, and technological systems operators. For example, if symptoms of fatigue, falling asleep, or fainting have been detected, an alarm signal would be triggered to stop the vehicle or device.[3] In addition, both military and civil aviation utilize systems for monitoring pilots to monitor their psychophysiological state,[4] ensuring pilot and passenger safety as well as the mission outcome, aircraft condition, and load being transported.

When monitoring seated individuals, the sensors and associated measuring equipment can be placed directly in the back or base of the seat, enabling monitoring without attaching electrodes or the recorder to the body.[5] On the other hand, special requirements are imposed on systems that must be able to operate in harsh environments without failing, such as high-temperature or high-humidity environments, which prevail in nonair-conditioned cockpits, and environments with high electromagnetic (EM) interference caused by radio or on-board radar systems.

Magnetic resonance imaging (MRI) examination presents another situation in which devices used for monitoring physiological parameters must be capable of operating in an environment with a strong EM field.[6,7] For example, monitoring changes in basic physiological parameters can enable the early detection of a claustrophobic episode, allowing the test to be immediately interrupted to remove the patient from unpleasant sensations.[8]

In this paper, the author justifies the need for monitoring basic physiological parameters in patients undergoing MRI scans, systematizes the knowledge of fiber-optic techniques purposed for recording life functions, which are potentially suitable for an MRI environment, and indicates the current directions of development in this area.

2 Importance of Monitoring the Patient During MRI

2.1 *Description of the MRI Environment*

The MRI environment is distinguished by high levels of magnetic induction density: 1.5 to 3.0 Tesla (T) in typical

*Address all correspondence to: Łukasz Dziuda, E-mail: ldziuda@wiml.waw.pl

appliances. However, systems achieving densities of 9.4 T or even 21.1 T have also been developed.[9,10] Strong penetration by the magnetic field is accompanied by high EM field strength, inducing radio frequency impulses. Conventional measuring equipment was not designed to work in such an environment.[11–13] Placing metal elements, which are common electronic components in typical recorders, in a strong magnetic field can induce eddy currents in these elements and cause them to heat up. This, in turn, can cause skin burns in patients.[14–16] Moreover, metal elements inside an MRI scanner affect the distribution of the EM field and could, therefore, impair the image quality. Additionally, the electrical signal transmitted by typical copper wires in conventional measurement equipment is sensitive to a strong EM field. As a result, the measured parameter information may be altered before reaching the MRI system operator, rendering the measurements unusable.

Optical sensors can provide an alternative solution for measurement equipment.[17,18] Because optical sensors are free from metal elements, they are fully penetrable by the EM radiation used in MRI and cause no interference.[19] Fiber-optic sensors[20–22] transmit signals using optical fibers, providing them with immunity to EM fields. Moreover, there are fiber-optic sensors[23] that are able to acquire a patient's physiological signals and subsequently extract the chosen parameters[24–28] if they are configured in an appropriate manner, i.e., connected with mechanical elements and placed near the patient.

2.2 *Episodes of Claustrophobic Reactions During MRI Examinations*

Along with computed tomography (CT), MRI has become one of the most common methods for detecting lesions in tissues.[29] Despite its high diagnostic efficiency and prospects for further advancement, e.g., functional magnetic resonance imaging, MRI has a major disadvantage because the patient must be placed in a narrow cylindrical tube for a few dozen minutes, which can induce claustrophobia or panic attacks. Furthermore, during brain scans, the patient's head is immobilized with a special collar, exacerbating the patient's discomfort. Attempts to minimize these reactions using open-type MRI systems have produced poor results. The patient's knowledge that the examination requires assuming a certain position for a length of time invades the patient's personal and mental space. As a result, an estimated 5 to 10% of patients undergoing an MRI experience high stress related to their restriction in the MRI chamber.[30,31] Moreover, 10% or more of all examinations using MRI cannot be commenced or completed due to claustrophobia.[32] The acute manifestation of anxiety symptoms immediately before or during MRI examinations can also occur in persons who have been taught anxiety and stress management techniques.[33] In the case of a 26-year-old man who was referred for an MRI due to back pain,[34] the MRI examination very likely contributed to the patient's development of posttraumatic stress disorder, which is, according to the Diagnostic and Statistical Manual of Mental Disorders (DSM-IV), an anxiety disorder caused by exposure to high stress.[35]

The reasons reported by patients for experiencing anxiety and (often) fear of MRI examinations include not only the space limitation and movement restriction, but also the high noise levels generated by the equipment, long duration of the examination, total isolation from the staff, and equipment that moves slowly toward the patient.[36,37] As many as 30% of patients undergoing MRI examinations experience mild symptoms of anxiety and stress. Such episodes usually result in the examination being stopped or extended. Moreover, these episodes may result in the administration of anxiolytics and sedatives to the patient, which is not always advised, possible, or safe.[32] Such actions may ultimately increase the examination cost as a result of the extended equipment use and involvement of additional medical and technical staff. Therefore, the early detection of anxiety or panic attacks is a significant issue in medicine and a considerable challenge for both equipment designers and all persons involved in examinations requiring any type of chamber, such as those employed in modern neuroimaging techniques.

2.3 *Basic Physiological Parameters and Their Link to Claustrophobia*

While a multipoint acquisition of physiological parameters, e.g., using a Holter-type system, is applied for diagnosis in hospitalized patients, the simple monitoring of basic vital functions is sufficient for persons monitored during regular activities. The respiration rate (RR), which specifies the number of ventilations per minute (vpm),[38] as well as the heart rate (HR), i.e., the number of heart beats per minute (bpm),[39] are basic physiological parameters. In general, RR is estimated using a respiration curve, while HR, coincident with pulse and heart rhythm, can be estimated based on an electrocardiogram, ballistocardiogram, or plethysmogram. Prophylactic examinations allow for the early detection of increased and/or irregular RR or HR, which can indicate emerging health disorders. Alarming trends in basic physiological parameters can justify a precautionary outpatient examination; likewise, similar trends observed during an MRI examination should lead to the completion or suspension of the examination and its adjustment in line with the current situation of the patient.

Respiration monitoring can be used to detect hyperventilation. Hyperventilation, i.e., an increased rate of pulmonary ventilation and considerably decreased depth of breathing, often leading to syncope,[40,41] is closely related to anxiety and panic disorders.[42,43] Breathing patterns in persons experiencing panic attacks are distinguished by high variability and irregularity.[44] Therefore, panic attacks can be predicted or monitored in terms of the course, intensity, and the speed at which the symptoms resolve.

One aspect in the study of hyperventilation concerns the mechanisms as well as physiological and psychological factors responsible for anxiety symptoms. In addition, conscious and controlled breath management has been analyzed for the treatment of various anxiety disorders. Because attempts to control and normalize breathing helped to reduce symptoms of anxiety and panic,[45] therapeutic programs have been developed to teach patients how to cope efficiently with hyperventilation during MRI examinations.[46]

The patient's heart function should also be measured during examinations[47] because HR indicators are considerably higher in persons suffering from general anxiety, panic, and hyperventilation in comparison with those who do not experience such discomfort. Therefore, that continuous, online monitoring of patients' circulatory parameters during MRI examinations will allow for the prediction and assessment of anxiety, panic, and claustrophobia closely related to the circumstances of examination.

Although patients likely to experience claustrophobic anxiety attacks are the most common group classified to be

monitored inside an MRI magnet, there are many other patient categories that require monitoring and support during MRI procedures. These are patients who are unable or may not be able to communicate or to use the alarm button:[7]

- neonatal and pediatric patients,
- sedated or anesthetized patients,
- disabled and insensible patients,
- patients in coma,
- patients with mental disorders,
- patients with impaired physiological functions,
- critically ill or high-risk patients,
- patients developing reactions to contrast media,
- patients with implanted pacemakers.

3 Fiber-Optic Sensors in the Measurement of Physiological Signals and Parameters

3.1 *Categorization of Monitoring Principles*

Most of the fiber-optic sensors[23,48–50] configured for delivering information on vital functions have been developed over the last 20 years and the results have been published in almost 100 papers.[41,51–145] Though only some of these sensors have been tested in an MRI environment, fiber-optic sensors are inherently immune to EM radiation and can be MRI-compatible. For these reasons, we consider all of the sensors discussed in the next section as potentially suitable for an MRI environment.

Forty-two fiber-optic sensors constructed by other groups[41,51–133] and five in-house-designed sensors[134–145] for monitoring vital signs can be easily classified into three major categories with several subcategories each, according to the location of the sensor application. In addition, we can distinguish seven sensor classes regarding the type of measurand as follows:

1. Sensors placed in (1a) a nostril or (1b) oxygen mask, measuring (I) humidity, (II) temperature, or (III) force of inhaled/exhaled air (flow);
2. Sensors embedded into (2a) expandable belts or (2b) special garments as well as affixed directly to (2c) the body, measuring (IV) the elongation/contraction, (V) strain (including curvature), or (VI) lateral pressure caused by respiration and/or heart work;
3. Sensors attached to (3a) the back of a chair, placed on/in/under (3b) a bed mattress, or embedded into (3c) a pneumatic cushion, measuring (V) the strain, (VI) pressure, or (VII) force caused by respiration and/or heart function.

Figure 1 illustrates this classification by showing the number of sensors in relation to the placement of the sensing element and the type of measurand. The largest groups are sensors embedded into a textile belt or bed mattress, which measure lung- and/or heart-induced elongation/contraction and strain, respectively.

To illustrate how trends in the area of fiber-optic sensors for recording physiological functions have changed over the last 20 years,[41,51–145] Fig. 2 shows the number of articles published in any individual year in each of the three categories. In the 1990s and at the beginning of the new millennium, the first devices placed in a nostril or oxygen mask were proposed. A significant development has occurred since the mid-2000s, when it was noted that the measuring elements could be embedded into wearable textiles, ensuring the immediate proximity of the sensors to the lungs and heart. However, due to the wide range of clothing sizes required to accommodate different patients, the interest in textile-based sensors has decreased in recent years. Wearable-textile sensors are now being replaced by sensors embedded into a bed or seat that do not require preparing the patient for monitoring. In addition to the literature review, the author describes his group's work on embedded sensors.[134–140,142–145]

3.2 *Results of Literature Review*

3.2.1 *Intensity-modulated fiber-optic sensors*

In recent years, different research groups have presented dozens of fiber-optic sensor designs suitable for use in an MRI

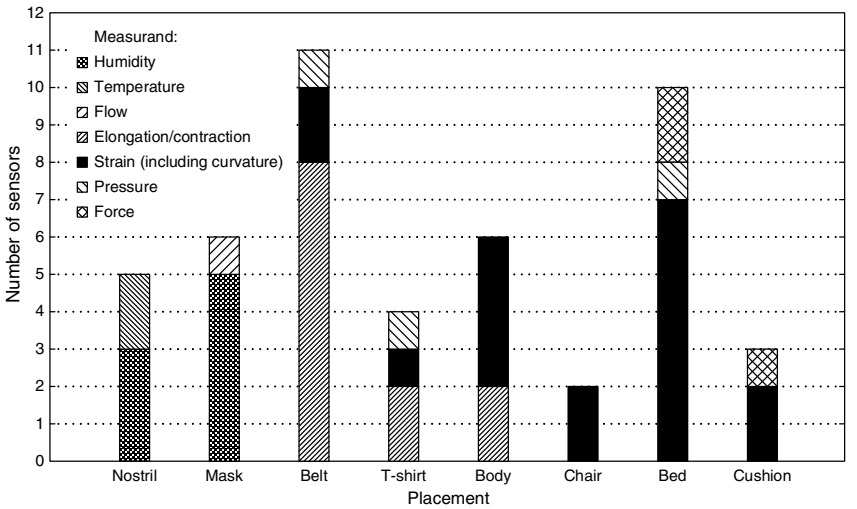

Fig. 1 Sensor classification depending on the placement of the sensing element and the type of measurand.[41,51–145]

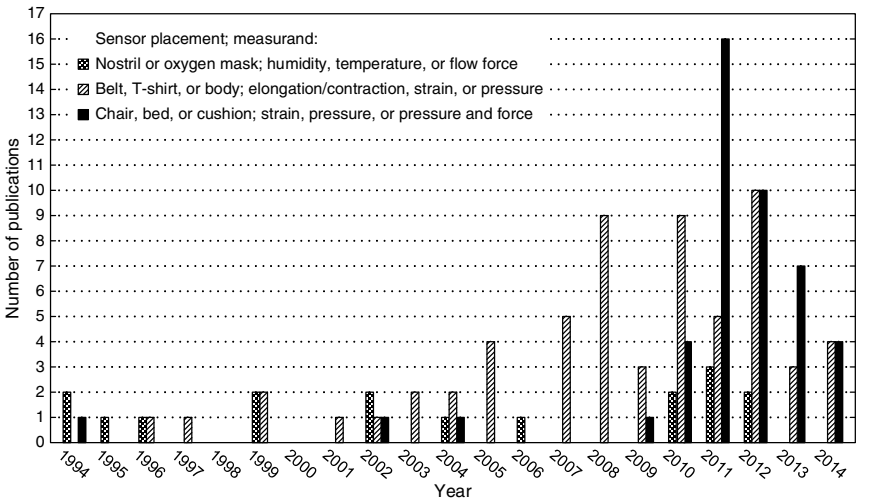

Fig. 2 Publishing activity in the field of fiber-optic sensors for monitoring vital signs.[41,51–145]

environment that allow the RR and/or HR to be obtained after processing the recorded signal. An RR-monitoring device that detected the evaporated humidity from the mouth and/or nose was one of the first sensors to be studied.[51–55] The condensed humidity substantially alters the interaction between the light from the optical fiber and the surrounding medium, which can be monitored by a photodetector. As shown in Fig. 3(a), during expiration, a water film (many hemispherical water drops) is formed at the optical fiber end with a refractive index >1, and the amount of light reflected back into the fiber decreases. During inspiration [Fig. 3(b)], the dry and cool air next to the fiber does not produce condensation at the tip. As the refractive index at the boundary approaches 1, the amount of light reflected back into the fiber increases. These changes in light reflection can be measured by a photodetector positioned at the opposite end of the optical fiber, and the RR can be monitored by counting the cyclic variations in the light reflection.

Table 1 lists the major properties of intensity-modulated fiber-optic sensors designed for monitoring respiration and/or heart function, which were studied in an MRI environment or are suitable for use in the presence of strong EM fields. In the first column, the category and subcategory of the sensor, according to above classification, are provided together with the reference paper(s) describing each of the mentioned devices. The second column presents the form of the sensor and the physiological parameter(s) that can be monitored. The third column summarizes the experimental studies and their results,

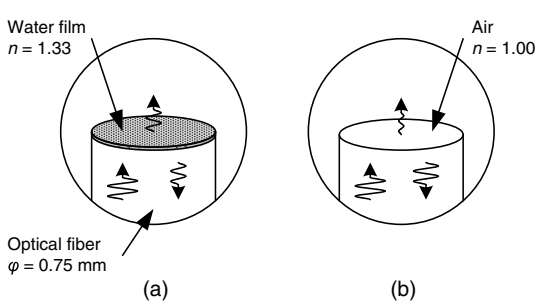

Fig. 3 Operation of an intensity-modulated fiber-optic sensor during (a) expiration and (b) inspiration.[51,52]

including the number of participants, testing procedure, and quantitative data on the sensor efficiency. The last column shows the MRI compatibility of the individual sensors verified at a given magnetic induction and/or for given imaging sequences.

3.2.2 *Interferometric fiber-optic sensors*

At the same time, solutions also emerged that were based on phase interferometry, where the optical signal that was directed to the measurement area of the optical fiber (placed near the monitored person, e.g., in the back or base of the seat) was compared with the output signal, which was modified by disrupting factors, such as respiration and heartbeats.[56–75] Body movements caused by the function of the lungs and heart cause phase changes between signals (sensing and reference) and could be identified as a series of time-variable interference patterns. Thus far, in research on the acquisition of physiological signals, fiber-optic interferometers have been tested in their most popular configurations, i.e., Michelson, Mach-Zehnder, and Sagnac interferometers.[58–60] The popular Michelson interferometer has been the most widely studied.[61–72] As shown in Fig. 4, the Michelson interferometer consists of two optical paths (arms), i.e., the sensing and reference fibers. Both fibers have mirrored ends, and the sensing region is formed by the differential path length between the two parallel fibers. Minute lung- and/or heart-induced changes in the sensing fiber length cause significant changes in the phases of reflected light, which subsequently produces changes in the optical power monitored by the photodetector and allows for the determination of RR and/or HR.

Human vital signs have also been monitored using fiber-optic speckle interferometry.[73–75] Speckle patterns can be observed in the laser light output of coherently illumined multimode fibers (MMFs), as shown in Fig. 5. The fiber output is projected onto a complementary metal-oxide semiconductor imaging sensor. Consecutive speckle images arise from the interference between propagating fiber modes and are highly sensitive to external fiber perturbations, such as those caused by the mechanical impact of human activity.

Recently, interferometric sensors have been developed in which a segment of photonic crystal fiber (PCF) was used as the measuring element.[76,77] As shown in Fig. 6, the collapsed region within the PCF allows the excitation and recombination

Table 1 Intensity-modulated fiber-optic sensors for respiration monitoring.

Category; reference	Sensing element; parameter	Characteristics of subjects; testing procedure; quantitative data on sensor efficiency	MRI compatibility
1a.I; [51–53]	Plastic tube; RR	10 healthy volunteers (M), age: 24 to 42 years; supine position, recording time: 100 breaths (each subject), normal ventilation (9 to 17 vpm); Wilcoxon test: no statistically significant differences between reference and measured RR values ($p > 0.05$), apnea and tachypnea: events detected immediately	Not tested
1a.I; [54]	As above	289 patients (151 M, 138 F), age: 8 to 90 years, mean 50.1 years; eight technicians estimated clinical utility of sensor: very valuable in 17 patients (5.9%), valuable in 77 patients (26.6%), not necessary in 195 patients (67.5%)	Yes (0.2 T, 1.0 T, and 1.5 T)
1a.I; [55]	As above	18 healthy volunteers, age: 9 to 83 years; recording time: 4×3 min periods (each subject), normal ventilation; t test: sensor significantly overestimated RR mean value ($p < 0.001$), 95% confidence interval: sensor did not overestimate number of breaths for individual registration (0.5 to 1.5 vpm, mean 14 vpm)	As above

Note: MRI, magnetic resonance imaging; RR, respiration rate; vpm, ventilations per minute.

of modes, thus creating an interferometer. The reflection spectrum of this device displays a sinusoidal interference pattern that instantly shifts when water molecules, which are present in exhaled air, are adsorbed on or desorbed from the PCF surface. Therefore, these sensors detect the difference between the humidity of inhaled and exhaled air, which allows a respiration curve and RR to be obtained.

A cornerstone for the development of the photonic crystal based interferometer was the Fabry-Pérot (FP) etalon interferometer shown in Fig. 7, which was formed by placing alternating multilayer thin films of polymers and inorganic nanoclusters on the cleaved end of a single-mode fiber (SMF).[78–80] However, the patient is required to wear a mask with built-in sensors, which presents a notable obstacle of the PCF- and FP-based fiber-optic interferometers for respiration monitoring. Table 3 lists the major results obtained using these devices.

The key advantage of interferometric methods is their high sensitivity; however, this can imply instabilities in the signal amplitude if the monitored person moves, changes his/her position, or simply coughs.[59,60] Then, the signal amplitude can reach relatively high values, which bring difficulties in the demodulation of the phase signal. Therefore, systems for the elimination or compensation of body movements are required, and advanced signal analysis techniques have to be able to detect miniature signal changes carrying information on respiration activity and heart function. Major outcomes obtained using these interferometric fiber-optic sensors for respiration and/or heart function monitoring are listed in Table 2, using a column layout identical to that presented in Table 1.

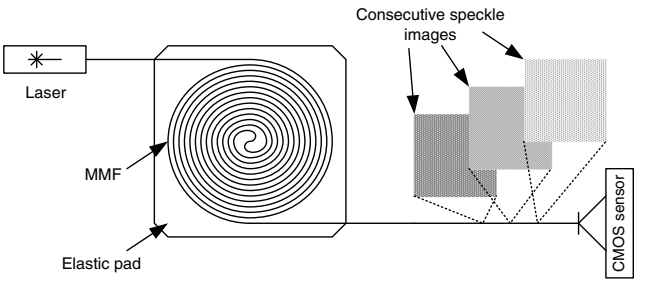

Fig. 5 Configuration of a fiber-optic speckle interferometer.

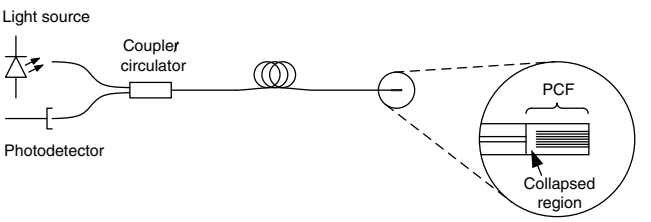

Fig. 6 Basic system with a photonic crystal fiber segment for monitoring breathing humidity.[76,77]

3.2.3 *Sensors in modalmetric configuration*

While the vital activity information is contained within the phase changes in fiber-optic interferometers, the so-called modalmetric configuration of a sensor detects the vibrations related to vital functions as light intensity modulations proportional to those

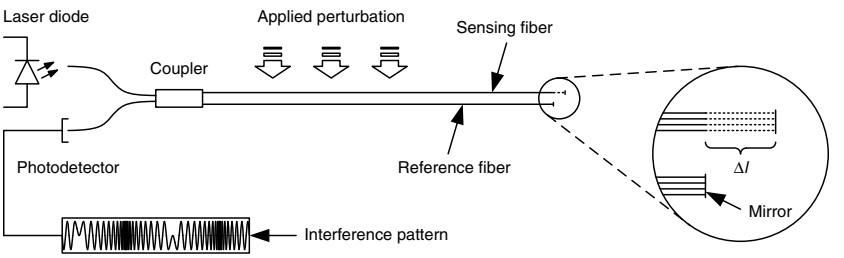

Fig. 4 Configuration of a fiber-optic Michelson interferometer.[61–69]

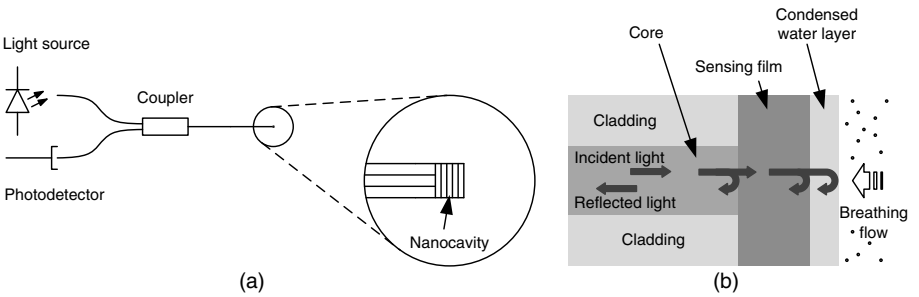

Fig. 7 Fabry-Pérot-based breathing sensor: (a) basic system and (b) sensing head.[79,80]

functions (sensor category: 3a.V).[60,81] Such sensors consist of (1) an SMF transmitting segment, (2) an MMF segment sensitive to mechanical stress, and (3) an SMF receiving segment, as shown in Fig. 8. The single-mode transmitting fiber delivers optical radiation to the MMF section, in which the layout of the mode field is dependent on mechanical deflections caused, for example, by respiration and heart function. In other words, the signal loss is primarily due to the bending loss when the MMF section is deformed. The amount of light reaching the single-mode receiving fiber reflects the layout of the mode

Table 2 Interferometric fiber-optic sensors for respiration and/or heart function monitoring.

Category; reference	Sensing element; parameter	Characteristics of subjects; testing procedure; quantitative data on sensor efficiency	MRI compatibility
2b.V; [56,57]	Mach-Zehnder, Michelson, or Sagnac interferometer embedded into elastic pad; RR or HR	No data (patent description)	Yes (no data)
3b.V; [56,57]	As above	As above	As above
3a.V; [58–60]	As above	Insufficient data	Not tested
3b.V; [61–72]	Michelson interferometer embedded into elastic mat; RR and HR	Several research sessions with varying numbers of participants and signal analysis techniques. Most recent experimental study: (1) rest: 20 healthy volunteers (19 M, 1 F), age: 31.0 ± 8.15 years; supine position, recording time: 60 s; sensitivity: 97.64 ± 7.28%, precision: 99.38 ± 2.80%, maximum relative error (MRE): 7.35 ± 7.20% for RR detection, sensitivity: 99.46 ± 1.11%, precision: 99.60 ± 1.05%, MRE: 3.16 ± 2.32% for HR detection; (2) cycling ergometer: 10 volunteers (9 M, 1 F), age: 31.30 ± 10.45 years, supine position, recording time: 60 s, sensitivity: 92.05 ± 6.10%, precision: 93.45 ± 3.08%, MRE: 16.28 ± 6.25% for RR detection, sensitivity: 96.22 ± 2.96%, precision: 95.35 ± 3.03%, MRE: 9.56 ± 3.67% for HR detection. In general, MRE: >30% for RR detection, <17% for HR detection	As above
3b.V; [73]	Speckle interferometer embedded into elastic mat; RR and HR	No data (patent description)	As above
3b.V; [74,75]	As above	Most recent experimental study: 10 healthy volunteers, age: 31.8 ± 8.1 years; rest, supine position, recording time: 120 s; sensitivity: 95.3 ± 3.0%, precision: 97.9 ± 2.3% for RR detection, sensitivity: 99.4 ± 0.6%, precision: 98.8 ± 1.5% for HR detection	As above
1b.I; [76]	Photonic crystal fiber interferometer inside capillary tube; RR	Two volunteers; sensor was tested for different conditions: normal breathing, accelerated breathing after physical exercise, stopped breathing for few seconds; basic evaluations only	As above
1b.I; [77]	As above	No information on number of participants and their age; sensor was tested for normal and irregular breathing; evaluation of sensor construction; no data on sensor efficiency	As above
1b.I; [78–80]	Fabry-Pérot interferometer inside plastic tube; RR	Tests were carried out using a simulated breathing flow system, with relation to thin-film refractive indices and thickness; no data on sensor efficiency	As above

Note: HR, heart rate.

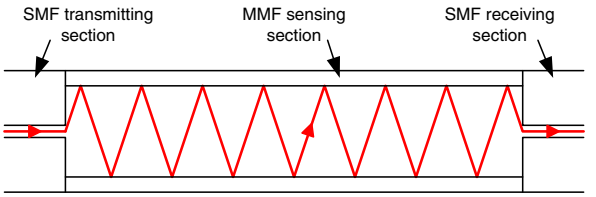

Fig. 8 Schematic layout of the mode field in the modalmetric sensor configuration.

field. Thus, the receiving section of the sensor serves as a detector for the radiation propagated within the MMF section, i.e., the measurement head. As described in the solutions involving interferometry, the measurement of vital functions with a modalmetric sensor is accomplished using ballistography.[60,81] The main disadvantage in the use of this type of sensor is that it is difficult to simultaneously record respiration and heart function. So far, no comprehensive evaluation of the modalmetric sensor has been performed in the MRI environment.

3.2.4 *Micro- and macrobending fiber-optic sensors*

In sensors measuring transmission loss caused by slight (miniscule) deflections of an optical fiber or in fiber bends with a radius of curvature well above the fiber diameter (>10 mm), i.e., in so-called micro-[82–88] and macrobend[89–107] sensors, respectively, the intensity of the light reaching the receiver is also measured. As in the cases described above, body movements (caused by respiration and heart function, among other things) are a complicating factor since these movements produce micro- and macrobends of fibers with a variable radius of curvature. Thus, along the axis of a bent fiber, the layout of the mode fields continuously changes as the energy radiates; this is seen in the form of light intensity changes at the receiver. The measuring system for micro- and macrobend sensors is distinguished by a simple design for the sensors alone as well as for the associated transceiver modules (light source and photodetector). Nevertheless, due to their relatively low sensitivity, the sensors have to be embedded in a special mat[82,83] or cushion,[85–88] on which the patient lies during monitoring, or in textiles, such as a vest, T-shirt, or belt, which are worn by the monitored person,[89–107] to ensure immediate proximity to the lungs and heart. An example of a microbend sensor system is shown in Fig. 9(a). The sensor mat is constructed by means of two microbenders with MMF passed between them, as shown in Fig. 9(b). The whole setup is covered with a textile material to protect the sensor. A macrobend sensor embedded into an expandable belt is illustrated in Fig. 10 in its most common arrangements, i.e., half-loop (half-oval-form), figure-eight loop, and U-shape.

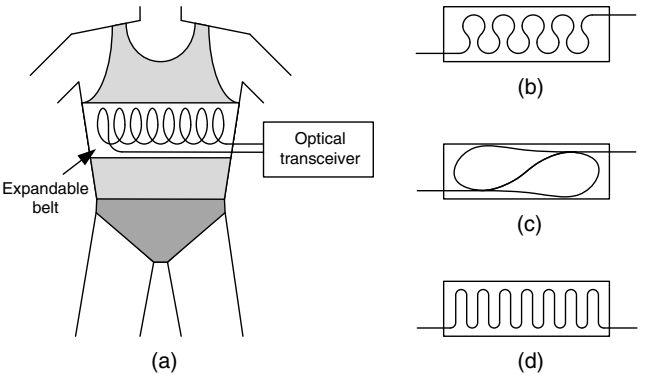

Fig. 10 (a) Macrobend sensor in an expandable belt. Arrangement of the optical fiber in the macrobend sensor: (b) half-loop, (c) figure-eight loop, and (d) U-shape.[92–107]

Another method for improving the sensitivity is the use of a standard MMF[41] or SMF[108] into which a short section of SMF with a narrower diameter core is inserted. In this hetero-core sensor segment, the transmitted beam is partially leaked into the cladding layer. Additionally, as shown in Fig. 11, the leaked light changes with the bending action of the hetero-core segment, and the bending property can be measured from the changes in transmission.

Table 3 characterizes the major properties of these micro- and macrobend fiber-optic sensors obtained during experimental studies.

3.2.5 *Plastic optical fiber-based sensors*

A variation of the microbend sensor is a system in which the intensity of light falling onto a plastic (polymer) optical fiber (POF) head is measured; this light was previously reflected from a mirror surface whose distance from the fiber front changes according to the respiration rhythm.[109] Figure 12(a) shows the structure of the abdomen-attached respiration sensor. The polymethyl-methacrylate (PMMA) tube fastens the aluminum mirror and one end of the spring, while the other end of the PMMA tube is attached to the POF tip.

Other solutions utilizing POF allow RR monitoring based on the temperature difference between inhaled and exhaled air[109,110] or the force with which the air is exhaled immediately in front of the nose or mouth.[111] In the first case, shown in Fig. 12(b), the intensity of the reflected light is changed upon the color variation of the temperature-sensing film, and the modulated light is guided to a photodetector via the POF link. In the second device, depicted in Fig. 12(c), the force of the exhaled air pushes a vertical flap, and the coupling of light from the fixed fiber becomes disturbed. The change in coupled power can be easily measured by a photodetector.

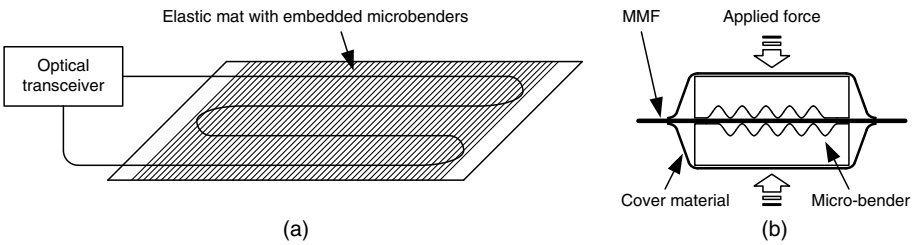

Fig. 9 Microbend fiber-optic sensor: (a) basic system and (b) microbender structure.[83,84]

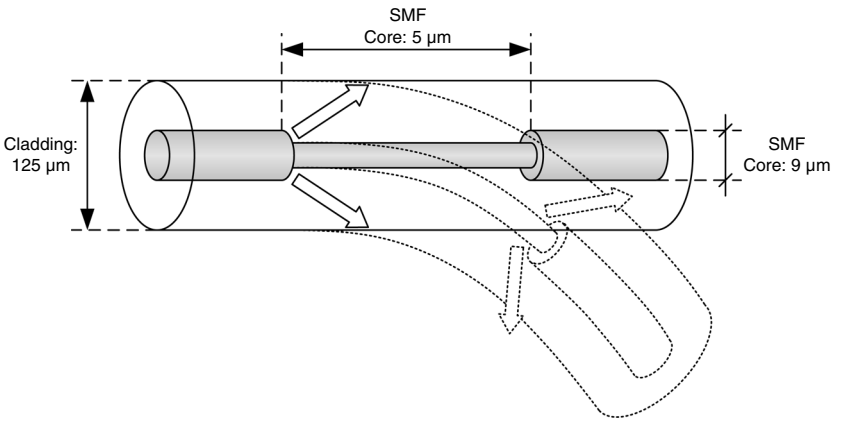

Fig. 11 Operation of a hetero-core fiber sensor.[108]

Breathing condition sensors also utilized POF as a substrate for the cladding layer, which swells when it comes into contact with water molecules within the exhaled air, as shown schematically in Fig. 13.[112,113] Under the dry-state conditions in Fig. 13(a), the refractive index of cladding layer, n_2, is slightly larger than that of the PMMA fiber core ($n_1 = 1.489$), and the sensor head is a leaky-type head. For the humid state in Fig. 13(b), the sensor head becomes a guided-type head as n_2 decreases, and the output light power, P_{out}, through the sensor head will increase remarkably, i.e., $P_{out2} > P_{out1}$.

Table 4 characterizes the major outcomes obtained using the above-mentioned POF-based sensors.

3.2.6 *Optical time domain reflectometry based sensors*

Another known solution is based on optical time domain reflectometry (OTDR), where the propagation of a light impulse (introduced into the POF and dispersed with partial reflection at the location of the mechanical disturbance of the fiber) is measured as a function of time (sensor category: 2a.IV).[96–101,114] Figure 14 illustrates a basic system employing a POF-OTDR-type sensor for respiration monitoring. The preliminary results show sufficient sensitivity for detecting respiratory movements, i.e., cyclic strain between 0 and 3%. Moreover, steps of 0.25% strain could be measured, demonstrating a quadratic correlation between the sensor signal and the applied strain. However, the sensor has not been evaluated in the MRI environment. The disadvantages of this type of sensor are a relatively low sampling rate for the signal and the need for complex and expensive transceivers.

The list of sensors allowing the acquisition of the respiration curve with the ballistocardiographic (BCG) signal is completed by solutions based on fiber Bragg gratings (FBGs) whose properties are described in the next section. The author also devotes Sec. 5.1 and 5.2 to explore the literature and present his work on FBG-based vital signs sensors, respectively.

4 Fiber Bragg Gratings

4.1 *Principle of Operation of FBG Sensors*

In recent years, FBGs have been the subject of much research and are some of the most widely utilized optical elements, serving a wide range of applications in telecommunications as well as in laser and measurement technology. The applications in which FBGs serve solely as sensors cover many fields,[146] e.g., the monitoring of structural health,[147–150] operating conditions of electrical plants,[151–153] or life processes in the human body.[26–28,154–158] Furthermore, FBGs are popular for their resistance to modulations in the optical signal intensity, which is possible because of the so-called spectral encoding, i.e., the information is contained not in the light intensity but in a spectral parameter (wavelength).[159] This property, along with its so-called self-reference capability, i.e., a return to the referential values of spectral parameters after achieving the initial conditions, allow multiple Bragg gratings to be contained within one optical fiber.[160,161] Exhibiting the standard advantages of fiber technologies, FBG-based sensors are immune to EM effects, chemically inert, small-scale, lightweight, and provide electrically safe modes of operation.[162,163]

A typical FBG sensor operates as a stop-band filter, where part of the light falling onto the grating is not retained but reflected. The Bragg grating is formed by a portion of the SMF core where periodic modulation is introduced in the refractive index value.[164] Beams of light reflected from individual grating layers, with the same phases, are subject to interference. This phenomenon occurs at only one wavelength, called the Bragg wavelength or the central wavelength, λ_B:

$$\lambda_B = 2n_{\text{eff}}\Lambda, \tag{1}$$

where n_{eff} is the effective refractive index,[165] and Λ is the modulation period of this index.

The spectrum of light reflected from the grating forms a pointed intensity peak, the maximum value of which is located at the Bragg wavelength, whereas the spectrum of light transmitted through the grating is a narrow intensity trough with its minimum value at the Bragg wavelength. An example of the signal reflected from a Bragg grating simulated using the T-matrix method[166–168] in Mathcad software is shown in Fig. 15. The simulated FBGs have the Bragg wavelength of 1550 nm with 4000 [Fig. 15(a)] or 12,000 [Fig. 15(b)] index modulation periods, which is equivalent to a grating length of 2 or 6 mm, respectively. The peak sharpness, full-width at half-maximum (FWHM), and the corresponding reflectance can be adjusted by the number of refractive index perturbations. In most sensor applications, the central wavelength is determined from the peak position because the shape of the reflected signal is easier to demodulate. Therefore, FBG-based sensors have one crucial advantage: they can be connected to a

Table 3 Micro- and macrobending fiber-optic sensors for respiration and/or heart function monitoring.

Category; reference	Sensing element; parameter	Characteristics of subjects; testing procedure; quantitative data on sensor efficiency	MRI compatibility
3b.VII; [82] and [83]	Sandwich microbender structure; RR	Most recent experimental study: 20 healthy volunteers (10 M, 10 F), age: 24 to 61 years; supine position, recording time: 30-min MRI session (each subject), normal ventilation (7 to 21 vpm); Pearson test: statistically significant correlation in reference and measured RR values ($p < 0.05$), accuracy: ± 2 vpm	Yes (1.5 T, spin-echo, T2-weighted)
3b.VII; [84]	Two microbenders embedded into elastic mat; RR and HR	Clinical trials: 11 healthy subjects (6 M, 5 F), age: 26 to 62 years; supine position, recording time: 30-min MRI session (each subject); Pearson test: good agreement in simultaneous RR and HR measurements between sensor and reference system, statistically significant correlations ($r = 0.963$, $p < 0.001$ for RR; $r = 0.997$, $p < 0.001$ for HR), maximum errors: ± 1.7 vpm for RR and ± 1.2 bpm for RR and HR	Yes (3.0 T)
3c.VII; [85–88]	Microbender array; HR	Several research sessions with different number of participants and various algorithms for signal analysis. Most recent experimental study: three volunteers, no age data; headrest position, recording time: 3×2 min periods; HR range: 69 to 72 bpm, error: <0.4 bpm	Not tested
2a.IV; [89] and [90]	Optical fiber; RR	Four piglets; tests aimed at monitoring chest wall motion during high-frequency oscillatory ventilation	As above
2a.IV; [91]	As above	Eight healthy volunteers (M), age: 25 to 56 years; sitting position, after 10 min rest, recording time: 3 to 4×1 min periods (each subject)	As above
2a.IV; [92–94]	Optical fiber in half-loop or figure-eight loop configurations; RR	Insufficient information on number of participants and research methodology; correlation coefficient: 0.7558	As above
2a.IV; [95–106]	Optical fiber in half-loop or U-shaped configurations; RR or HR (at apnea)	Four volunteers, waistline range: 80 to 110 cm; sensor was tested for different conditions: normal breathing, slow and deep breathing, stepping on ledge, filling dishwasher; elongations of the abdominal circumference: <1%	Yes (no data)
2b.VI; [107]	Optical fiber in half-oval-form geometry; RR	One volunteer (M), age: 28 years; Four custom-made optical fibers were tested in five placements and with three types of breathing: diaphragmatic, upper costal, and mixed breathing; respiration-induced signal amplitude: max 60 mV_{0-pk}	Not tested
1b.I; [41]	Hetero-core fiber-optic arrangement (core: 50-3-50 μm); RR	One volunteer; recording time: 30 s, sensor was tested with five types of respiration: breathing by mouth, by nose, heavily, deeply, not breathing	As above
3b.VI; [108]	Hetero-core fiber-optic arrangement (core: 9-5-9 μm) embedded inside plastic sheet with eight sensing elements; RR	Seven volunteers; during sleep, recording time: >6 h (each subject), sensor was tested for different breathing conditions, e.g., apnea, and various configurations of single sensing elements	As above

Note: bpm, beats per minute.

transceiver with a single fiber cable. This means that the sensor can be connected using only one of its terminals.

4.2 *Strain and Temperature Sensitivity of FBGs*

The FBG susceptibility to strain, which is manifested as a shift of the Bragg wavelength, $\Delta\lambda_B$, motivated our first FBG sensor model for monitoring respiration and heart function. The Bragg shift[148,169] has the following relationship:

$$\frac{\Delta\lambda_B}{\lambda_B} = \left\{1 - \frac{n_{\text{eff}}^2}{2}[p_{12} - \nu(p_{11} + p_{12})]\right\}\Delta\varepsilon = (1 - \rho_e)\Delta\varepsilon, \tag{2}$$

where p_{11} and p_{12} are the photoelasticity coefficients of silica (fiber core), v is Poisson's coefficient, $\Delta\varepsilon$ is the strain change, and ρ_e is the effective photoelasticity coefficient. When a 1550-nm-wavelength light is injected into the FBGs inscribed into the

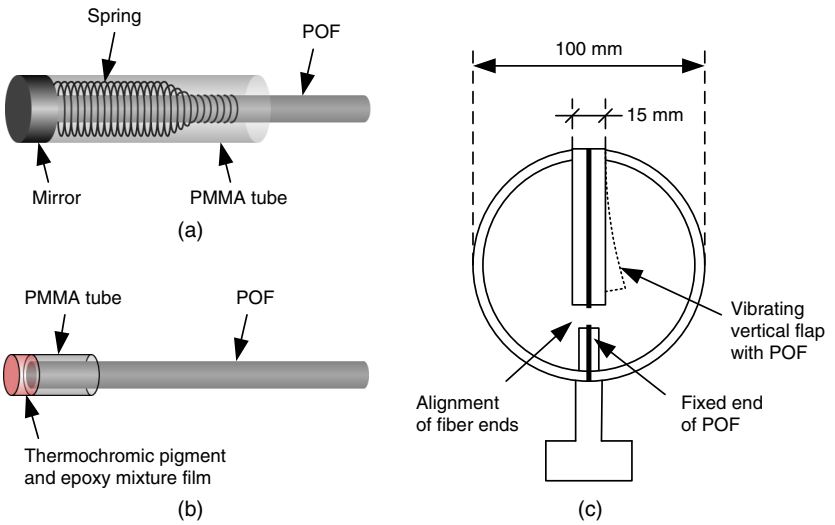

Fig. 12 The plastic (polymer) optical fiber (POF)-based sensors for detecting (a) abdominal respiratory movements, (b) humidity, and (c) temperature of the exhaled air.[109,111]

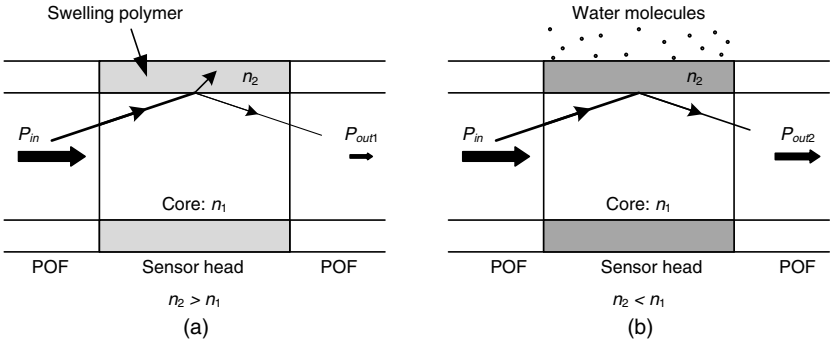

Fig. 13 Operation of a POF-type breathing sensor in the (a) dry state and (b) humid air.[113]

core of a germanium (Ge)-doped fiber, the effective elasticity coefficient is 0.218.[169] The strain change, expressed in the units of microstrain ($\mu\varepsilon$), is given by:[168,170]

$$\Delta\varepsilon = \frac{\Delta\lambda_B}{k_\varepsilon}, \tag{3}$$

where the FBG strain responsivity, k_ε, is 1.212 pm/$\mu\varepsilon$.

Due to the phenomenon of thermal expansion, the Bragg wavelength is also affected by temperature changes, ΔT, as follows:

$$\frac{\Delta\lambda_B}{\lambda_B} = (\alpha + \zeta)\Delta T, \tag{4}$$

where α and ζ are the thermal expansion and thermo-optic coefficients, respectively. Typically, α ranges from 0.54 to 0.55×10^{-6}/°C, while ζ usually ranges from 8.3 to 8.6×10^{-6}/°C for the Ge-doped silica fiber core.[150,153,171–173] Therefore, for a wavelength of 1550 nm, the temperature change is given by:

$$\Delta T = \frac{\Delta\lambda_B}{k_T}, \tag{5}$$

where the FBG temperature responsivity, k_T, is ~13.7 pm/°C.[150,174,175] Due to the considerable difference between the fiber diameter (125 μm for common optical fibers) and the FBG length (5 to 10 mm for a standard grating inscribed in an SMF core), the effects of the fiber diameter are assumed to be negligible. Finally, the expected strain- and temperature-induced wavelength shift of an FBG can be calculated as follows:

$$\Delta\lambda_B = k_\varepsilon\Delta\varepsilon + k_T\Delta T. \tag{6}$$

4.3 *Mathcad Simulations*

As the heart and lungs work, deformations occur on the surface of the torso, which can be measured by strain gauges, such as FBG sensors. Preliminary testing with an FBG applied to the chest near the heart showed that heartbeats cause peak-to-peak strains with values not less than 4 $\mu\varepsilon$. At the same time, breathing-induced strains were detected at least four times greater than the heart beats, i.e., $>16\,\mu\varepsilon_{\text{pk-pk}}$. These values were taken as the amplitudes of the BCG signal and the respiration curve, respectively, to demonstrate how the working heart and lungs affects the Bragg wavelength when an FBG makes physical contact with the subject's torso. Figures 16–18 show the results of simulations performed using Mathcad software. Figure 16 demonstrates changes in the Bragg wavelength caused only by cardiac function, e.g., during apnea. The upper graph

Table 4 The plastic (polymer) optical fiber based sensors for respiration monitoring.

Category; reference	Sensing element; parameter	Characteristics of subjects; testing procedure; quantitative data on sensor efficiency	MRI compatibility
2a.IV; [109]	PMMA tube; RR	Insufficient data	Yes (0.32 T, spin-echo T1-weighted, gradient-echo T2-weighted)
1a.II; [109] and [110]	Thermochromic-pigment applied on PMMA tube; RR	As above	As above
1a.II; [110]	Silver halide applied on PMMA tube; RR	As above	As above
1b.III; [111]	Sensor head; RR	No information on number of participants and their age; sensor was tested for normal breathing, evaluations of several sensor designs; maximum sensitivity: 1.2 vpm at resolution >1 Hz	Not tested
1b.I; [112] and [113]	Hydroxyethylcellulose and polyvinylidenefluoride-based sensor head; RR	No information on number of participants and their age; sensor was tested for normal breathing disturbed by coughs, basic evaluations of the sensor construction, response time: <1 s	As above

Note: PMMA, polymethyl-methacrylate.

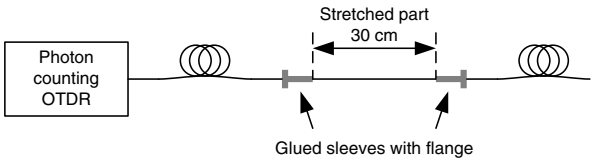

Fig. 14 Basic system with a POF optical time domain reflectometry type sensor for detecting respiration.[96]

shows a 1-s window (2-s window shown in the still image) representing the animated curve of the heart-induced strain during the 30-s measurement duration. The signal was obtained by the superposition of several sine functions whose amplitudes and periods were chosen so that the resultant signal shape was similar to a ballistocardiogram.[176,177] In other words, the BCG signal expressed in microstrains with a 4-$\mu\varepsilon$ amplitude and 1-s period (60 bpm) is presented in the upper graph. The middle graph shows the strain-induced Bragg wavelength shifts of the FBG peak synchronized with the strain changes. To facilitate the calculation, the reflected spectrum is represented by a Gaussian with a reflectance close to 1 and with an FWHM of ~0.1 nm. The lower graph demonstrates how changes in the heart-induced strain modulate the Bragg wavelength in time. The axes are intentionally inverted to emphasize synchronization with the middle graph. Moreover, this result reveals that the maximum value of the FBG reflected spectrum could be used for drawing the ballistocardiogram shape in wavelengths. According to Eq. (3), the strain-induced wavelength shift changes linearly with the heart-induced strain, hence the heart-induced Bragg wavelength shift.

Figures 17 and 18 show the same BCG signal additionally supplemented with the effects of breathing and temperature changes, respectively. The videos are presented in a similar convention as Fig. 16, except that the upper graph in Fig. 18 shows a 5-s window representing the animated curve of the heart- and lung-induced strain along with the temperature trace (rate

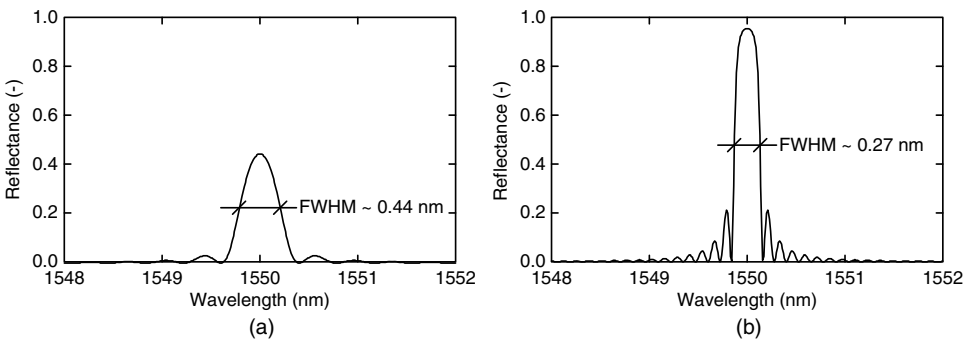

Fig. 15 Reflected spectrum simulated using the T-matrix method for (a) 2-mm fiber Bragg grating (FBG) and (b) 6-mm FBG.

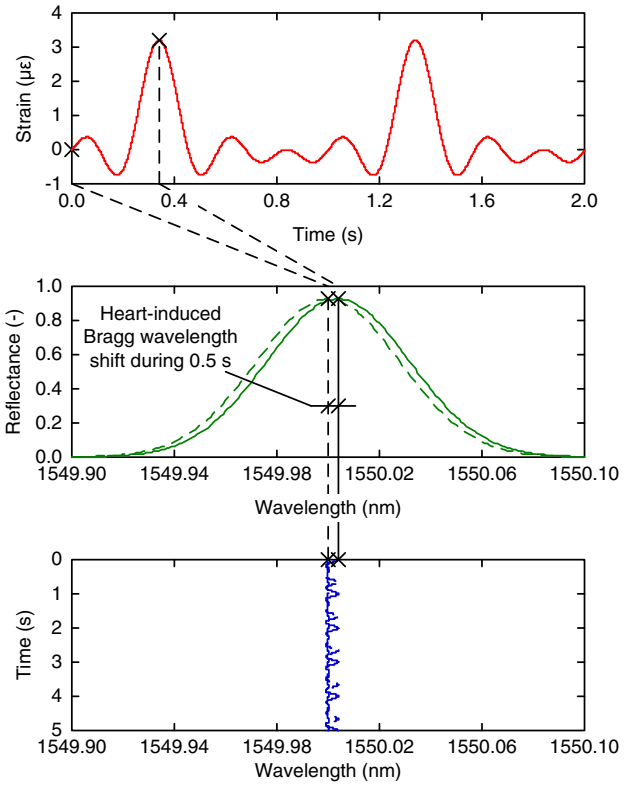

Fig. 16 Demonstration of Bragg wavelength shift with heart-induced strain (MOV, 2.51 MB) [URL: http://dx.doi.org/10.1117/1.JBO.20.1.010901.1].

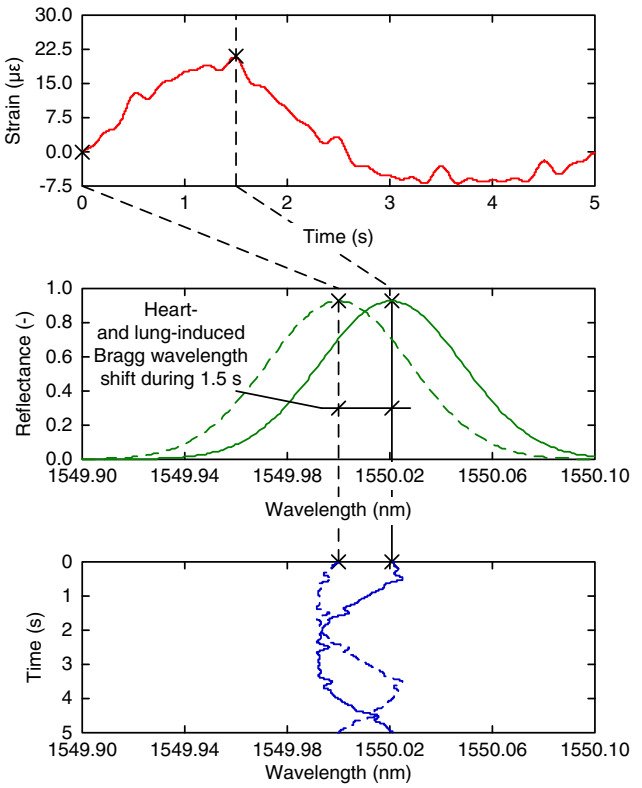

Fig. 17 Demonstration of Bragg wavelength shift with heart- and lung-induced strain (MOV, 2.36 MB) [URL: http://dx.doi.org/10.1117/1.JBO.20.1.010901.2].

increase of 1°C/s). The characteristic shape for the breathing signal was obtained using a superposition of the sine function and its second harmonic. The resultant signal has a 16 $\mu\varepsilon$ amplitude and 5-s period (12 vpm). Finally, the ballistocardiogram and respiration curve signals are superposed to form the time-varying trace of the strain exerted on the FBG sensor. Fig. 18 clearly shows that gradual heating of the grating does not disturb the measurement of heart- and lung-induced strain because the temperature growth influences the mean value of the measured wavelength (signal), whereas the heart- and lung-induced vibration causes changes to the instantaneous value. The temperature-induced drift can be removed by appropriate signal processing, and hence, further considerations could treat the effects associated with temperature fluctuations without affecting the heart- and lung-induced Bragg wavelength shift measurements.

5 FBG-Based Sensors for Monitoring Vital Signs

5.1 *Literature Exploration*

The literature provides a number of descriptions in which a single FBG[115–118] or multiple FBGs[97–106,114,119–123] act as the main sensing elements for acquiring body movements caused by respiratory and/or heart function. In both cases, FBGs can be embedded in the clothing worn by the patient during monitoring [97–106,115–122] or mounted in the bed on which the person lies, as shown in Fig. 19.[123]

Furthermore, FBGs are used as sensors for detecting sounds produced by a working heart.[124,125] Preliminary studies of long-period gratings (LPGs), a variation of Bragg gratings, for

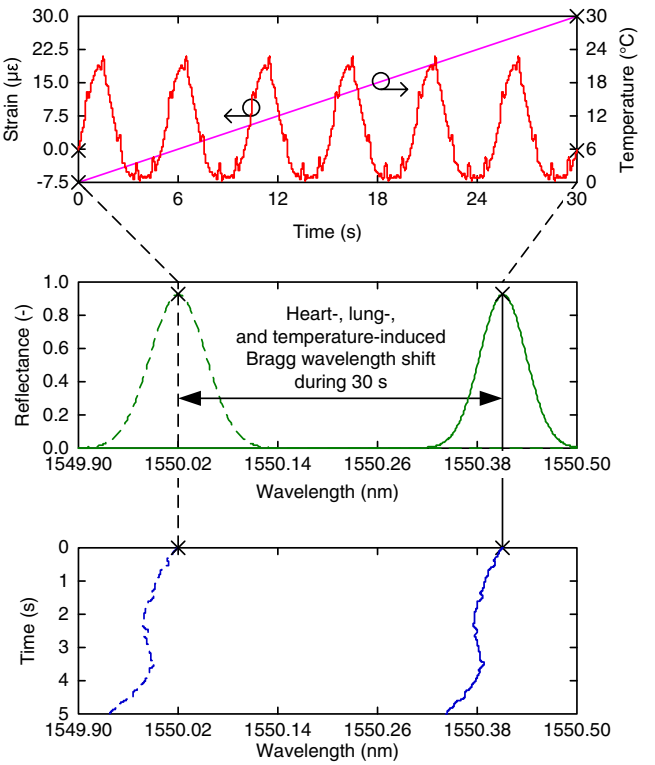

Fig. 18 Demonstration of Bragg wavelength shift with heart- and lung-induced strain as well as a temperature increase of 30°C (MOV, 2.11 MB) [URL: http://dx.doi.org/10.1117/1.JBO.20.1.010901.3].

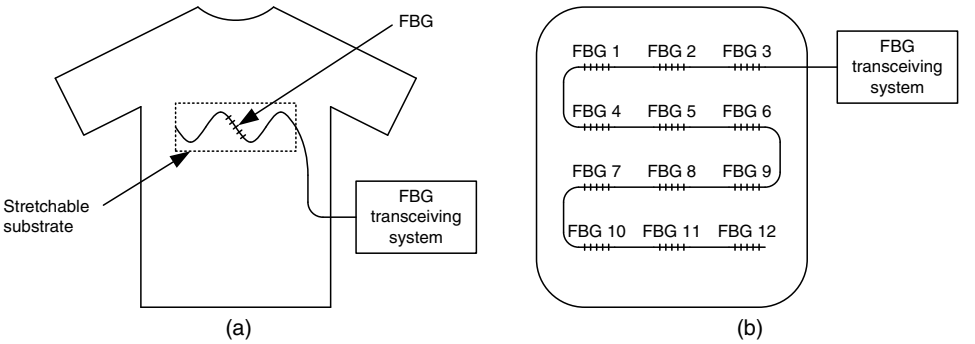

Fig. 19 Sample locations of FBGs: (a) single sensing element sewn in a T-shirt[116] and (b) bed sensor array.[123]

recording ventilatory movements and/or volumes have been performed because these gratings are particularly sensitive to any deformations in the LPG section.[126–132] Change in thorax curvature is sensed as bending of an LPG attached to the thorax. Bending induces strain and stress across the fiber and, in consequence, a change in its refractive index via the strain-optic effect, which manifests as a change in position, shape and amplitude of resonant bands in the transmission spectrum. The cladding modes generated by an LPG are more affected by bend-induced refractive index changes across the fiber than the back-propagating core modes generated by an FBG. Until recently, complex and expensive transceiving systems were used to handle LPG-based sensors, although the latest studies present a monochromatic measurement scheme that requires only a photodiode as a detector.[132] Moreover, a fiber LPG curvature sensing scheme has been presented lately as a system capable for detecting the mechanical motions and/or sounds of the human heart from surface of the torso.[133] Table 5 lists the major properties of FBG-based sensors for respiration and/or heart function monitoring. In general, fiber gratings provide many benefits with relatively few disadvantages, therefore, these elements have been of interest to the author for application to physiological measurements.

5.2 *Development of In-House-Designed Sensors*

5.2.1 *Prototype sensors*

The preprototype sensor base was formed by a pneumatic cushion, which served as a medium for transmitting strains caused by the movements of the person leaning against or lying on the cushion.[134–137] As shown in Fig. 20, an FBG attached inside the cushion records the strains in the form of instantaneous Bragg wavelength changes. The strains can be calibrated to represent the respiration curve and ballistocardiogram. Adequate signal filtration allows reading of RR and HR.

The commercially available sm130-700 four-channel device by Micron Optics[178] was used as a transceiver system, which is also called the interrogation system or interrogator, and was equipped with a broadband light source and a tunable FP filter allowing the 1510 to 1590 nm band to be scanned at a frequency of 1 kHz. This interrogation system type is one of the most popular methods for analyzing the reflected FBG spectrum. The measurement is performed by placing a peak from the FBG (or several peaks from an array of FBGs) within the free spectral range, i.e., within the interval between successive interference maxima of the FP filter, and monitoring the changes in the Bragg wavelength by means of spectral tuning, as shown in Fig. 21. The peak-to-peak resolution of the sm130-700 interrogator is 1 picometer (pm), which, upon conversion according to Eq. (3), ensures dynamic measurement of the strain changes $\Delta\varepsilon$ with a resolution of 0.8 $\mu\varepsilon_{\text{pk-pk}}$.

The initial sensor tests were conducted to assess whether the magnitude of the respiration- and heart-function-induced strains is sufficient for detection in the signal from the FBG-based sensor. The evaluation was performed at a test facility, where the monitored person sat in an office chair with a firm back. The sensor (cushion) was placed between the back of the monitored person and the back of the chair at heart height. In all recorded cases, the signal consisted of two fundamental components according to the simulations presented earlier: a slowly changing wave reflecting lung function, i.e., the respiration curve, and cyclic disturbances to this curve reflecting heart activity, i.e., the ballistocardiogram. As shown in Fig. 22(a), the signal wave amplitude was within 20 to 30 $\text{pm}_{\text{pk-pk}}$, which corresponds to strain values of 16.5 to 24.8 $\mu\varepsilon_{\text{pk-pk}}$. The heart function disturbed the signal envelope with an amplitude of ~10 $\text{pm}_{\text{pk-pk}}$, corresponding to a strain of 8.3 $\mu\varepsilon_{\text{pk-pk}}$. A clear upward trend in the signal indicates the temperature increase of the FBG element due to the proximity of the subject's body. In order to demonstrate that the sensor can simultaneously obtain RR and HR, the signal was subjected to parabolic detrending and Fourier transform. Figure 22(b) shows the Fourier spectrum in which two peaks at frequencies of 0.35 and 1.45 Hz are easily observable. They correspond to the RR (21 vpm) and HR (87 bpm), respectively. An additional peak at 2.90 Hz reflects the sinusoidal component of the BCG signal with a frequency twice higher than the HR. The magnitude increase toward zero frequency (constant component) indicates deficiencies in signal detrending.

Given that the preprototype sensor was an *ad hoc* design for initial laboratory evaluation, we subsequently designed improved versions. The optimization work was based on modeling in the SAP2000 environment. Using the finite element method (FEM),[179] we analyzed how individual sensor component parameters influenced the quality of the signal obtained. Numerical models were developed to analyze the effects of different dimensions, thicknesses, and cushion wall rigidity as well as the effects of several varieties of adhesives (considering the adhesive layer thickness, Young's modulus, and thermal expansion coefficient when set) on the sensor properties. In this manner, another cushion-based prototype sensor[137–139] and its simplified version using an elastic plate as the medium for transferring the strains to the measuring element[137,140] were constructed. Additionally, a special stethoscope with a built-in FBG,

Table 5 The fiber Bragg grating (FBG) based sensors for respiration and/or heart function monitoring.

Category; reference	Sensing element; parameter	Characteristics of subjects; testing procedure; quantitative data on sensor efficiency	MRI compatibility
2a.V; [115]	Single FBG; RR	One volunteer (M), 26-year old; sitting position, during rest, sensor was tested for different conditions: slow and deep breathing, fast and shallow breathing	Not tested
2b.IV; [116] and [117]	Single FBG embedded into polymeric foil; RR and HR	12 healthy volunteers, age: 20 to 30 years; standing position, during rest, sensor was tested when the subjects breathed naturally and when they stopped breathing for few seconds, recording time: 60 s, respiration-induced Bragg wavelength shift amplitude: max 153 pm_{pk-pk}, heartbeat-induced Bragg wavelength shift amplitude: max 12 pm_{pk-pk}	As above
2a.IV; [118]	Single FBG; RR	No information on number of participants and research methodology; respiration-induced Bragg wavelength shift amplitude: max 60 pm_{pk-pk} (according to graphical data), designers concentrated mainly on signal processing	Yes (no data)
2a.VI; [119]	Two FBGs written in Er-doped fiber, laser cavity fixed to plastic plate; RR	Two healthy volunteers (M), age: 26 and 24 years; sensor was tested in four conditions, including normal breathing (mean: 12.60 and 19.32 vpm for first and second volunteer, respectively), breath apnea, breath in different gestures (sitting and standing), and breath recovery procedure after strenuous activity, recording time: 60 and 210 s; elongation ratio for the flexible textile: 15 and 9% (first subject with waistline: 78 cm)	Not tested
2a.IV; [97–106], [114], [120], and [121]	Several FBGs; RR and HR	Healthy adult volunteers, sensor was tested for normal breathing and when breath was stopped for a few seconds; elongations of the abdominal circumference: 1 to 3%, respiration-induced Bragg wavelength shift amplitude: max 152 pm_{pk-pk}, heartbeat-induced Bragg wavelength shift amplitude: max 25 pm_{pk-pk}	Yes (no data)
2b.IV; [122]	Array of 40 FBGs; three-dimensional volumetric changes of the human torso	Five volunteers, age: 27 to 56 years, waistline range: 73.7 to 96.5 cm; no information on recording time; mean Pearson coefficient for correlation in the reference and measured volume values: 0.86 ± 0.03 ($p < 0.01$), maximum volumetric error: 15%	Not tested
3b.V; [123]	12 FBGs (3×4 array), arc-shaped metal bridges; RR	10 subjects, no age data; supine position, no information on recording time, the sensor was tested for normal breathing (10 to 25 vpm); maximum error: ± 1 vpm when compared with manual counting	As above
2c.IV; [124]	Single FBG, stethoscope structure; HR	Sensor was attached on speaker membrane emulating heart sounds; heartbeat sound-induced Bragg wavelength shift amplitude: max 10 pm_{pk-pk}, proof-of-concept demonstration only	As above
2c.V; [125]	Single FBG; blood flow and HR	FBG was fixed to speaker emulating the effect of blood flow-induced wrist motions; amplitude of heartbeat spectrum: 5 dB higher than the floor (poor selectivity), preliminary demonstration only	As above
2c.V; [126] and [127]	Array of sensing platforms consisted of two LPGs (each), flexible pad; RR	Sensor was tested at five different localizations on resuscitation training manikin; respiration-induced Bragg wavelength shift amplitude: max 3.18 pm_{pk-pk}, depending on the change in the torso circumference	As above
2a.V; [128–131]	LPG-based curvature sensor array, flexible band; RR	Six volunteers (M), age: 29 to 65 years, different body dimensions with marked variation in body shape; standing position, recording time: 5×1 min periods that consisted of typically 10 breaths (each subject); maximum volumetric error: 6% when compared with spirometer	As above

Table 5 (*Continued*).

Category; reference	Sensing element; parameter	Characteristics of subjects; testing procedure; quantitative data on sensor efficiency	MRI compatibility
2c.V; [132]	Single LPG; volumetric changes of the human torso	18 healthy volunteers (9 M, 9 F), age: (33 ± 8) years, BMI: (24 ± 5) kg/m^2; supine position, recording time: not less than 30 s (each subject), natural and shallow breathing (typical tidal volumes: 400 to 800 ml); minute volume error: (8.7 ± 4.4) % for natural breathing, (10.1 ± 5.8) % for shallow breathing, when compared with a spirometer, paired *t* test: no statistically significant differences between the minute volumes measured by the sensor and spirometer, mean tidal volume error: (10.5 ± 3.8) % for natural breathing, (15.0 ± 4.8) % for shallow breathing, good agreement between the mean tidal volumes measured by the two methods	As above
2c.V; [133]	3 or 4 LPGs attached to the human torso; motion of the heart wall next to the apex region of the heart	2 subjects, age: 34 and 43 years., chest diameter: 87 and 113 cm, respectively; neutral spine position, no information on recording time; sensor were tested at 6 different locations on the human torso, seismocardiographic signals up to 54 Hz were obtained, the sensing scheme can resolve individual components of the mechanical wave generated by the human heart revealing common frequencies of 1.3, 7.6, 10.8, and 22.1 Hz present in tests on both subjects	As above

Note: LPG, long-period grating.

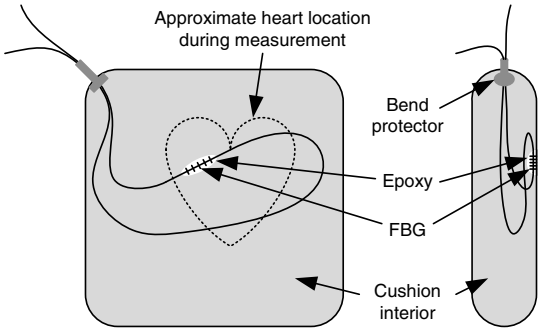

Fig. 20 The FBG location inside the cushion: top and side view.

enabling the monitoring of vibrations caused by the function of the cardiovascular system, e.g., in the cervical artery region, was designed as the source of the reference signal.[135–139,141]

5.2.2 *MRI-compatible sensor*

The experiences discussed above allowed us to design an FBG sensor suitable for MRI environments. The development of the sensor was preceded by FEM simulations to determine the deflection lines that react to heart and lung movements.

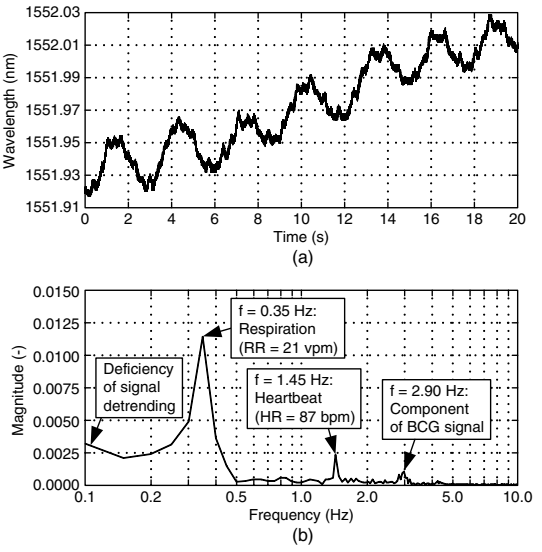

Fig. 22 The sensor ability to obtain the respiration rate (RR) and heart rate (HR) simultaneously: (a) a 20-s portion of a recording with visible respiration wave with cyclic heart-induced disturbances and temperature drift and (b) the Fourier spectrum of the above-shown signal.

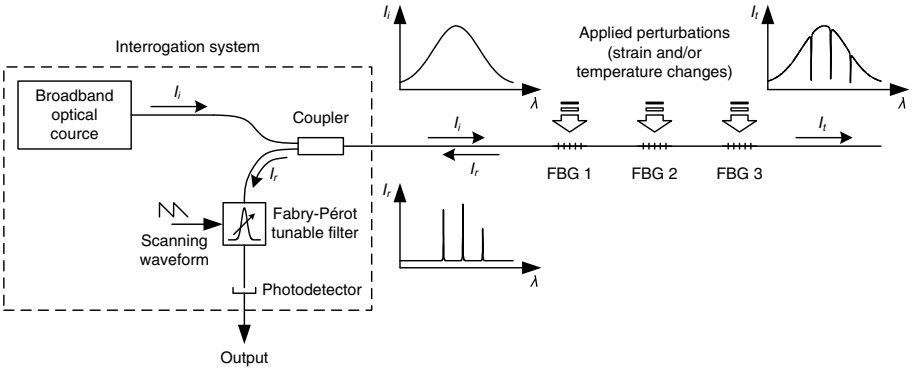

Fig. 21 The FBG interrogation system based on a tunable filter.

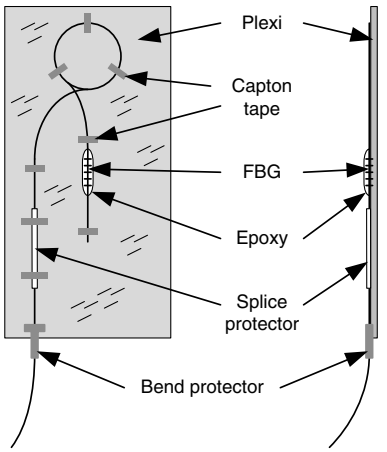

Fig. 23 The magnetic resonance imaging (MRI) compatible sensor construction.

Theoretical results obtained from FEM simulations and confirmed with laboratory tests have shown a trade-off between highly accurate parameter measurements and the comfort of the monitored person. An elastic plate with larger dimensions provides a better transfer of body vibrations and, thus, produces greater amplitudes due to the extraction/contraction of the FBG measuring element. Nevertheless, the large sensor dimensions require a thicker plate to prevent it from being cracked under the pressure exerted by a larger body surface, which impairs the comfort of the monitored person. On the other hand, a smaller, thinner plate allows the sensor to be placed on a thin, adequately profiled mattress on the MRI scanner track table, providing comfort for the monitored person.

Thus, in the MRI-compatible sensor, a Perspex plate with dimensions of 95×220 mm and a thickness of 1.5 mm was used.[140,142–145] A single FBG was attached to the central part of the plate (along the longitudinal axis) by a thin layer of epoxy adhesive that exhibited considerable rigidity when set and had a thermal expansivity coefficient comparable to that of the glass used in the fiber. The sensor structure is shown in Fig. 23. One of the FBG terminals was spliced with a 10-m optical fiber terminated with an ferrule connector/angled physical contact connector. The fiber splice protector was fitted with a ceramic strengthening core instead of the standard (steel) core. The redundant fiber between the FBG and the splice protector was formed into a multiturn loop and attached to the plate.

Before performing experiments on the FBG sensor in its natural working conditions, the frequency response of the measuring system was determined, and the signals within the BCG band, i.e., 1 to 20 Hz,[65,180] were recorded without a loss in quality.[144] The BCG band was observed well below the sensor's resonance frequency, which was confirmed when the numerical modeling results were obtained.

The research on the sensor was performed in an Achieva 1.5-T MRI scanner chamber by Philips,[181] which was available at the Military Institute of Aviation Medicine, Warsaw, Poland. As depicted in Fig. 24(a), the sensor was placed in the mattress of the MRI scanner track table in a position under the patient's back near the heart. The sensor output signal was transmitted from the scanner to the interrogator located in the MRI system operation room via a 10-m fiber-optic cable running through a wall opening. The signals were visualized online and archived in a database using a portable computer that was also located in the operation room [Fig. 24(b)] and connected to the interrogation system.

To acquire the reference respiration curve and electrocardiographic (ECG) signal, we used modules of different patient monitoring systems, such as Precess 3160 by Invivo,[182] which were designed to operate in the MRI environment. The respiration and ECG signals were obtained using pneumatic bellows and carbon electrodes, respectively, attached to patient. The data were transmitted wirelessly from the modules to the computer using a 2.4-GHz radio link. Figure 25 demonstrates

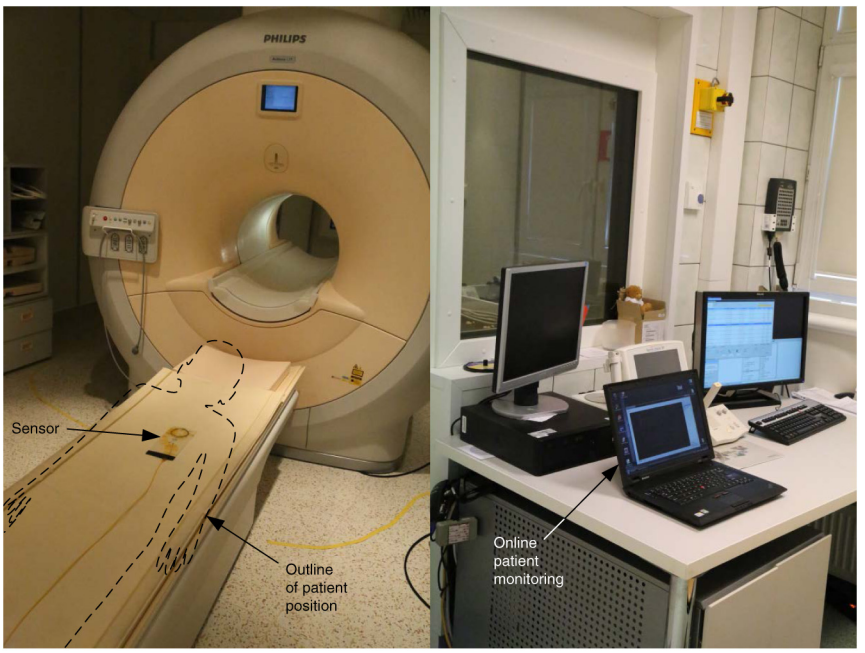

Fig. 24 Location of (a) the sensor and (b) the computer for visualization of monitoring results in the MRI system.

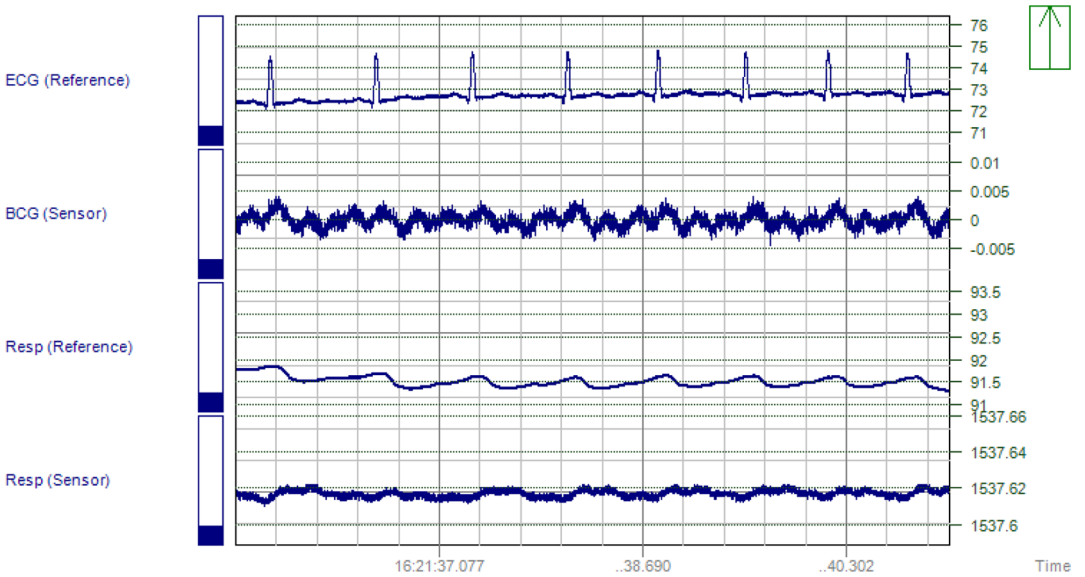

Fig. 25 Example of recording vital signs during a magnetic resonance imaging (MRI) scan (MOV, 11.4 MB) [URL: http://dx.doi.org/10.1117/1.JBO.20.1.010901.4].

an example of the recorded respiration and heart activity using the FBG-based sensor and the patient monitor, obtained during an MRI scan. The BCG signal was obtained by subjecting the source signal to band filtering in the range of 2 to 60 Hz, which did not eliminate the physiological information carried in the signal. As shown in Fig. 25, the reference signals are clearly better than the signals from the fiber-optic sensor. This results from resolution limitations of the interrogation system as well as the susceptibility to loss of contact between the monitored person and the sensor based on a single FBG. Regarding the first of the mentioned shortcomings, only a few solutions may offer slightly better resolution than the interrogator used, but this usually results in a reduced scanning speed.[183,184] High-speed systems that are not commercially available have also been proposed.[185–187] On the other hand, the sensor reliability can be easily improved through the multiplexing of FBGs, acquiring signals from several different places of the body, addressing all the FBGs with one optical fiber, and handling such an arrangement with one interrogation unit.

The experiments consisted of two phases: (1) a pilot study, in which 5-min intervals of MRI examinations of the spine were recorded where the sensor's center of symmetry was placed in the region of the vertebrae Th2 and Th3[144] and (2) clinical research, in which full imaging of the thoracic spine (vertebrae Th1 to Th12) was recorded for several tens of minutes.[145] The pilot study was used to analyze the images obtained with magnetic resonance and demonstrate that the MRI system EM radiation fully penetrated the sensor. Another goal was to confirm that the sensor did not affect the monitored person and to determine whether the sensor worked normally in a magnetostatic field at an induction level of 1.5 T as well as in gradient magnetic fields and pulse-modulated EM fields. Twelve healthy volunteers participated in the pilot research. Tests in a real MRI environment showed that the sensor was safe for the monitored person and did not affect the quality of imaging. In particular, the sensor did not introduce artifacts into the spin echo imaging sequence in T1- and T2-weighted times or into the gradient echo sequences in T2-weighted times. Moreover, the results showed that the optical signal delivered by the sensor was not adversely impacted by the high EM field strength.

The second phase of the experiments determined if it would be possible to utilize the FBG-based sensor for lengthy measurements of the mechano-physiological signals for a patient lying on the sensor and to examine the possible impact of the sensor on the patient's comfort during a full MRI examination. The clinical research was performed with three patient-volunteers who underwent standard MRI examinations of the thoracic

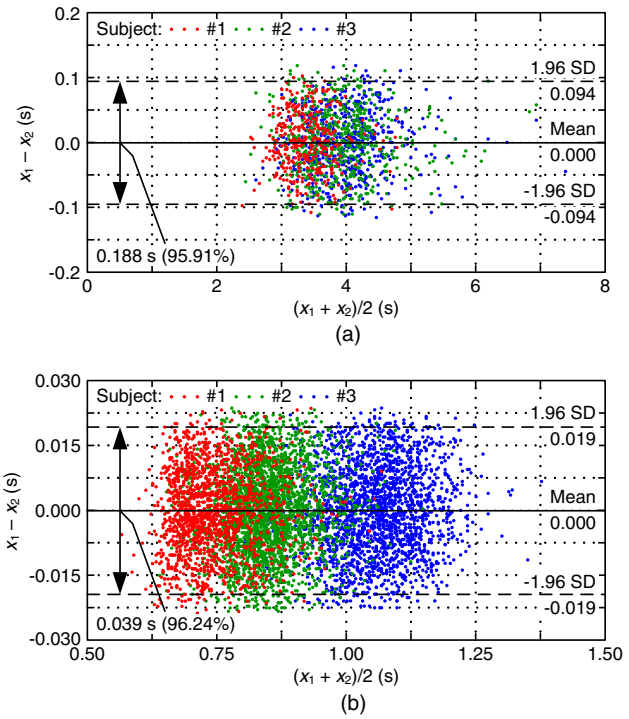

Fig. 26 Bland-Altman assessment for the specification capability of characteristic points used in determining (a) RR and (b) HR; $(x_1 - x_2)$ means the differences between the times of occurrence of the successive characteristic points of the sensor and reference signals; $(x_1 + x_2)/2$ means the averages of the times of occurrence of the successive characteristic points of the sensor and reference signals.

Table 6 In-house-designed fiber-optic sensors for respiration and heart function monitoring.

Category; reference	Sensing element; parameter	Characteristics of subjects; testing procedure; quantitative data on sensor efficiency	MRI compatibility
3c.V; [134–137]	Single FBG; RR and HR	Seven healthy volunteers, age: 26 to 39 years; during rest, sitting position, recording time: 60 s (each subject); respiration-induced Bragg wavelength shift amplitude: max 30 pm_{pk-pk} (24.8 $\mu strain_{pk-pk}$), heartbeat-induced Bragg wavelength shift amplitude: max 10 pm_{pk-pk} (8.3 $\mu strain_{pk-pk}$), relative error: <14% for HR detection	No (metallic parts)
3c.V; [137–139]	Two FBGs; RR and HR	Seven healthy volunteers, age: 25 to 37 years; during rest after physical exercises, sitting position, recording time: 10 min (each subject); respiration-induced Bragg wavelength shift amplitude: max 150 pm_{pk-pk} (124 $\mu strain_{pk-pk}$), heartbeat-induced Bragg wavelength shift amplitude: max 10 pm_{pk-pk} (8.3 $\mu strain_{pk-pk}$), relative error: <12% for HR detection	As above
3b.V; [137] and [140]	Two FBGs; RR and HR	The most recent experimental study includes two phases during rest: (1) standing position, one healthy volunteer (M), age: 36 years; recording time: 120 s; relative error: max 6.55% for HR detection; (2) sitting position, one healthy volunteer (F), age: 26 years; recording time: 120 s; relative error: max 6.24% for HR detection	Yes (not tested)
2c.IV; [135–139] and [141]	Single FBG, stethoscope structure; HR	Sensor was coupled with speaker membrane emulating heart sounds; heartbeat sound-induced Bragg wavelength shift amplitude: 5 pm_{pk-pk}, frequency range: 25 to 135 Hz, amplification: 9.2 dB at 100 Hz	No (metallic parts)
3b.V; [140] and [142–145]	Single FBG; RR and HR	Two phases during MRI examination: (1) pilot studies, 12 healthy volunteers (8 M, 4 F), age: 33.25 ± 6.06 years; recording time: 5 min (each subject); relative error: <7% (MRE: 5.24 ± 1.02%) for RR detection, <6.5% (MRE: 5.71 ± 0.61%) for HR detection; (2) clinical studies, 3 healthy volunteers (2 M, 1 F), age: 31.33 ± 5.03 years; total recording time: 95 min 25 s; relative error: max 7.67% for RR detection, max 6.61% for HR detection	Yes (1.5 T, spin-echo T1- and T2-weighted, gradient-echo T2-weighted)

spine. No problems were reported in relation to the operation of the sensor during MRI. None of the examined patients complained of discomfort related to the presence of the sensor under his/her back during a 40-min examination.

The results of these experiments on the sensor showed that the maximum errors calculated with respect to the reference values of the respiration curve and ECG signal did not exceed 8% for RR and 7% for HR. The Bland-Altman method[188,189] was applied to statistically assess the accuracy of specifying characteristic points used in determining RR and HR, i.e., the local maxima of the respiration curve (source signal) and the local maxima of the ballistocardiogram (filtered signal), respectively. In the first case, the times of occurrence of the successive characteristic points were compared with the times of occurrence of the successive local maxima of the referential respiration curve. In the second case, the times of occurrence of the successive characteristic points were compared with the times of occurrence of the successive R waves of the ECG signal. Interpretation of the Bland-Altman analysis, shown in Fig. 26, shows that this method exhibits no systematic error. For the entire data set (clinical research, three subjects), the sensor demonstrates good reproducibility. The agreement range limits are as narrow as 0.188 and 0.039 s, and 95.91 and 96.24% of the sample values lie within the limits when specifying characteristic points needed for the RR and HR determination, respectively. Moreover, the error is not proportional and does not depend on how frequently the characteristic points occur.

The RR and HR measurements obtained with this FBG sensor demonstrated that its accuracy was comparable for all examined persons. The detailed results of these experiments in the MRI environment are presented elsewhere.[142–145] In addition to the BCG measurements obtained in the supine position, measurements were also recorded for sitting and standing persons.[140] The major properties of the in-house-designed sensors are listed in Table 6.

6 Summary and Conclusions

This paper provides an overview of fiber-optic sensors for recording physiological signals caused by mechanical movements of the lungs and heart for sensors discussed in the literature and those studied by the author. Moreover, we focus on FBGs, a special group of optical elements, whose unique properties make them ideal for applications in harsh environments, including the EM radiation-saturated MRI environment. In the literature, fiber grating-based sensors are the most frequently reported devices for recording life functions. However, comparatively strong competitors are micro- and macrobend sensors due to their simple design and ease of signal demodulation. Numerous publications have also reported on interferometric sensors, which are unbeatable in terms of precision but require complex signal processing techniques. Other fiber-optic

measurement methods have been explored to a much lesser extent, and the small number of publications has provided poor data.

The need to monitor basic vital functions and relate these measurements to the patient's emotional state during an MRI examination has been noted by many researchers,[190] who have further stressed that claustrophobia symptoms should be detected as early as possible.[191] New heart rate variability techniques based on the ECG signal make it possible to assess the activity of the autonomic nerve system in an accurate and reliable manner.[192] In this area, sensors employing FBGs can play an important role because, if properly configured, they can record RR and HR of the patient through body movements caused by respiratory and heart function.

In contrast to other groups working on optical fiber sensors for monitoring vital functions, [41,51–133] in our research,[140,142–145] we show that noninvasive, simultaneous acquisition of the respiration curve and BCG signal for a patient undergoing an MRI examination is possible with a single FBG. This method's originality and usefulness are illustrated by the fact that it is not necessary to use any textiles to ensure immediate proximity of the lungs and heart to the sensor. Therefore, there is no need to perform any additional actions to prepare the patient for monitoring, which may require additional medical staff. During the course of our work, we have shown that the FBG-based sensors are safe for patients in the chamber of a working MRI scanner and that the sensor has no impact on the quality of the imaging. This type of sensor can also be used during CT scans, where there are no similar demanding requirements arising from the presence of a magnetic field, but where respiration and heartbeat should be continuously monitored.[193] Recently, this sensor has been applied in research on claustrophobia disorders with a specific focus on hyperventilation for persons undergoing MRI and CT examinations.

Acknowledgments

The research work presented in this article was part of Project No. UDA-POIG.01.03.01-14-136/08, supported in part by the resources of the EU's European Regional Development Fund under the Innovative Economy Operational Programme 2007–2013, and this research has been continued within Project No. DOBR/0052/R/ID1/2012/03, financed by the resources of the Program for National Defense and Security, Poland.

References

1. N. Oliver, F. Flores-Mangas, and R. de Oliveira, "Towards wearable physiological monitoring on a mobile phone," in *Mobile Health Solutions for Biomedical Applications*, P. Olla and J. Tan, Eds., pp. 208–243, IGI Global, Hershey, New York, NY (2009).
2. A. Müller et al., "Remote monitoring in patients with pacemakers and implantable cardioverter-defibrillators: new perspectives for complex therapeutic management," in *Modern Pacemakers—Present and Future*, M. K. Das, Ed., pp. 147–166, InTech, Rijeka, Croatia (2011).
3. B.-G. Lee and W.-Y. Chung, "Driver alertness monitoring using fusion of facial features and bio signals," *IEEE Sens. J.* **12**(7), 2416–2422 (2012).
4. A. Marques et al., "Light aviation and flight safety: monitoring system for unpressurised cabins. Flight and physiological data acquisition," 2012, http://www-sre.wu.ac.at/ersa/ersaconfs/ersa12/e120821aFinal00856.pdf (28 December 2014).
5. Ł. Dziuda, F. Skibniewski, and W. Torbicz, *Non-Contact Methods for Monitoring Psychophysiological Activity: Selected Papers*, Akademicka Oficyna Wydawnicza EXIT, Warszawa, Poland (2011).
6. F. G. Shellock, S. M. Myers, and K. J. Kimble, "Monitoring heart rate and oxygen saturation with a fiber-optic pulse oximeter during MR imaging," *AJR Am. J. Roentgenol.* **158**(3), 663–664 (1992).
7. Shellock R & D Services, Inc. and F. G. Shellock, "Monitoring patients in the MRI environment," 2012, http://www.mrisafety.com/SafetyInfov.asp?SafetyInfoID=186 (28 December 2014).
8. I. Eshed et al., "Claustrophobia and premature termination of magnetic resonance imaging examinations," *J. Magn. Reson. Imaging* **26**(2), 401–404 (2007).
9. T. Vaughan et al., "9.4 T human MRI: preliminary results," *Magn. Reson. Med.* **56**(6), 1274–1282 (2006).
10. C. Qian et al., "A volume birdcage coil with an adjustable sliding tuner ring for neuroimaging in high field vertical magnets: ex and in vivo applications at 21.1 T," *J. Magn. Reson.* **221**, 110–116 (2012).
11. M. Folke et al., "Critical review of non-invasive respiratory monitoring in medical care," *Med. Biol. Eng. Comput.* **41**(4), 377–383 (2003).
12. F. Q. Al-Khalidi et al., "Respiration rate monitoring methods: a review," *Pediatr. Pulmonol.* **46**(6), 523–529 (2011).
13. T. Niendorf, L. Winter, and T. Frauenrath, "Electrocardiogram in an MRI environment: clinical needs, practical considerations, safety implications, technical solutions and future directions," in *Advances in Electrocardiograms—Methods and Analysis*, R. M. Millis, Ed., pp. 309–324, InTech, Rijeka, Croatia (2012).
14. S. Jones, W. Jaffe, and R. Alvi, "Burns associated with electrocardiographic monitoring during magnetic resonance imaging," *Burns* **22**(5), 420–421 (1996).
15. M. F. Dempsey and B. Condon, "Thermal injuries associated with MRI," *Clin. Radiol.* **56**(6), 457–465 (2001).
16. H. Kugel et al., "Hazardous situation in the MR bore: induction in ECG leads causes fire," *Eur. Radiol.* **13**(4), 690–694 (2003).
17. Y. Takemura, J. Sato, and M. Nakajima, "A respiratory movement monitoring system using fiber-grating vision sensor for diagnosing sleep apnea syndrome," *Opt. Rev.* **12**(1), 46–53 (2005).
18. S. J. Cala et al., "Chest wall and lung volume estimation by optical reflectance motion analysis," *J. Appl. Physiol.* **81**(6), 2680–2689 (1996).
19. ICT Results, "Optical sensors make MRI scans safer," Science Daily, 20 September 2008, http://www.sciencedaily.com/releases/2008/09/080918091609.htm (28 December 2014).
20. I. H. Yellowlees, "Fibreoptic sensors in clinical measurement," *Br. J. Anaesth.* **67**(1), 100–105 (1991).
21. A. G. Mignani and F. Baldini, "In vivo biomedical monitoring by fiber-optic systems," *IEEE J. Lightwave Technol.* **13**(7), 1396–1406 (1995).
22. L. G. Lindberg, H. Ugnell, and A. Oberg, "Monitoring of respiratory and heart rates using a fibre-optic sensor," *Med. Biol. Eng. Comput.* **30**(5), 533–537 (1992).
23. K. T. V. Grattan and T. Sun, "Fiber optic sensor technology: an overview," *Sens. Actuator A Phys.* **82**(1–3), 40–61 (2000).
24. A. G. Mignani and F. Baldini, "Biomedical sensors using optical fibres," *Rep. Prog. Phys.* **59**, 1–28 (1996).
25. A. G. Mignani and F. Baldini, "Fibre-optic sensors in health care," *Phys. Med. Biol.* **42**(5), 967–979 (1997).
26. M. A. Zawawi, S. O'Keeffe, and E. Lewis, "Intensity-modulated fiber optic sensor for health monitoring applications: a comparative review," *Sens. Rev.* **33**(1), 57–67 (2013).
27. F. Taffoni et al., "Optical fiber-based MR-compatible sensors for medical applications: an overview," *Sensors* **13**(10), 14105–14120 (2013).
28. P. Roriz et al., "From conventional sensors to fibre optic sensors for strain and force measurements in biomechanics applications: a review," *J. Biomech.* **47**(6), 1251–1261 (2014).
29. *Magnetic resonance imaging (MRI) equipment—a global strategic business report*, Global Industry Analysts, Inc., San Jose, CA (2013).
30. J. C. Meléndez and E. McCrank, "Anxiety-related reactions associated with magnetic resonance imaging examinations," *J. Am. Med. Assoc.* **270**(6), 745–747 (1993).
31. L. M. Harris, J. Robinson, and R. G. Menzies, "Predictors of panic symptoms during magnetic resonance imaging scans," *Int. J. Behav. Med.* **8**(1), 80–87 (2001).
32. F. T. Tschirch et al., "Low-dose intranasal versus oral midazolam for routine body MRI of claustrophobic patients," *Eur. Radiol.* **17**(6), 1403–1410 (2007).

33. R. Lukins, I. G. P. Davan, and P. D. Drummond, "A cognitive behavioural approach to preventing anxiety during magnetic resonance imaging," *J. Behav. Ther. Exp. Psychiatry* **28**(2), 97–104 (1997).
34. S. E. Lakhan, "3T MRI induced post-traumatic stress disorder: a case report," *Int. Arch. Med.* **5**(1), 27 (2012).
35. American Psychiatric Association, *Diagnostic and Statistical Manual of Mental Disorders, Fourth Edition: DSM-IV-TR*, American Psychiatric Publishing, Washington, DC (2000).
36. S. A. Sarji et al., "Failed magnetic resonance imaging examinations due to claustrophobia," *Australas. Radiol.* **42**(4), 293–295 (1998).
37. S. Wright, "All embracing," *Nurs. Stand.* **19**(50), 32–33 (2005).
38. S. R. Braun, "Respiratory rate and pattern," in *Clinical Methods: The History, Physical, and Laboratory Examinations*, H. K. Walker, W. D. Hall, and J. W. Hurst, Eds., pp. 226–230, Butterworth Publishers, Stoneham, MA (1990).
39. A. H. Roscoe, "Assessing pilot workload. Why measure heart rate, HRV and respiration?," *Biol. Psychol.* **34**(2–3), 259–287 (1992).
40. P. Várady et al., "A novel method for the detection of apnea and hypopnea events in respiration signals," *IEEE Trans. Biomed. Eng.* **49**(9), 936–942 (2002).
41. S. Akita, A. Seki, and K. Watanabe, "A monitoring of breathing using a hetero-core optical fiber sensor," *Proc. SPIE* **7981**, 79812W (2011).
42. A. E. Meuret et al., "Voluntary hyperventilation in the treatment of panic disorder—functions of hyperventilation, their implications for breathing training, and recommendations for standardization," *Clin. Psychol. Rev.* **25**(3), 285–306 (2005).
43. C. L. Badour et al., "Specificity of peritraumatic fear in predicting anxious reactivity to a biological challenge among traumatic event-exposed adolescents," *Cognit. Ther. Res.* **36**(4), 397–406 (2012).
44. M. Grassi et al., "Baseline respiratory parameters in panic disorder: a meta-analysis," *J. Affect. Disord.* **146**(2), 158–173 (2013).
45. D. Rosenfield et al., "New breathing therapy reduces panic and anxiety by reversing hyperventilation" (2010) http://www.sciencedaily.com/releases/2010/12/101220200010.htm.
46. E. Wollburg, W. T. Roth, and S. Kim, "Effects of breathing training on voluntary hypo- and hyperventilation in patients with panic disorder and episodic anxiety," *Appl. Psychophysiol. Biofeedback* **36**(2), 81–91 (2011).
47. A. Pittig et al., "Heart rate and heart rate variability in panic, social anxiety, obsessive-compulsive, and generalized anxiety disorders at baseline and in response to relaxation and hyperventilation," *Int. J. Psychophysiol.* **87**(1), 19–27 (2013).
48. E. Udd, "An overview of fiber-optic sensors," *Rev. Sci. Instrum.* **66**, 4015 (1995).
49. B. Lee, "Review of the present status of optical fiber sensors," *Opt. Fiber Technol.* **9**(2), 57–79 (2003).
50. S. Yin, P. B. Ruffin, and F. T. S. Yu, *Fiber Optic Sensors*, 2nd ed., CRC Press, Boca Raton, FL (2008).
51. M. Vegfors et al., "Presentation and evaluation of a new optical sensor for respiratory rate monitoring," *Int. J. Clin. Monit. Comput.* **11**(3), 151–156 (1994).
52. P. A. Oberg et al., "Evaluation of a new fiber-optic sensor for respiratory rate measurements," *Proc. SPIE* **2331**, 98–109 (1995).
53. H. Pettersson et al., "Optical aspects of a fibre-optic sensor for respiratory rate monitoring," *Med. Biol. Eng. Comput.* **34**(6), 448–452 (1996).
54. C. Larsson et al., "Respiratory monitoring during MR imaging. The clinical value of a new fibre-optical monitor," *Acta Radiol.* **40**(1), 33–36 (1999).
55. C. Larsson and P. Staun, "Evaluation of a new fibre-optical monitor for respiratory rate monitoring," *J. Clin. Monit. Comput.* **15**(5), 295–298 (1999).
56. D. Varshneya and J. L. Maida, "Fiber-optic monitor using interferometry for detecting vital signs of a patient," U.S. Patent No. 6498652 (2002).
57. D. Varshneya, J. L. Maida, and L. A. Jeffers, "Fiber-optic interferometric vital sign monitor for use in magnetic resonance imaging, confined care facilities and in-hospital," U.S. Patent No. 6816266 (2004).
58. M. Życzkowski and B. Uziębło-Życzkowska, "Human psychophysiology activity monitoring methods using fiber optic sensors," *Proc. SPIE* **7838**, 78380W (2010).
59. M. Życzkowski et al., "Interferometric fiber optics based sensor for monitoring of the heart activity," *Acta Phys. Pol. A* **120**(4), 782–784 (2011).
60. M. Życzkowski, "The measurement of respiration and heart work using fiber-optic sensors," in *Non-Contact Methods for Monitoring Psychophysiological Activity: Selected Papers*, Ł. Dziuda, F. Skibniewski, and W. Torbicz, Eds., Akademicka Oficyna Wydawnicza EXIT, Warszawa, Poland (2011).
61. S. Šprager, D. Đonlagić, and D. Zazula, "Monitoring of basic human vital functions using optical interferometer," in *Proc. of 10th IEEE Int. Conf. on Signal Processing*, Vol. 2, pp. 1738–1741, Institute of Electrical and Electronics Engineers, New York, NY (2010).
62. S. Šprager, D. Đonlagić, and D. Zazula, "Estimation of heart rate, respiratory rate and motion by using optical interferometer as body sensor," in *Proc. of the 13th Int. Conf. on Signal and Image Processing*, pp. 280–287, ACTA Press , Anaheim, California (2011).
63. S. Šprager, D. Đonlagić, and D. Zazula, "Heart beat monitoring using optical interferometric signal and pseudo Wigner-Ville distribution," in *Proc. of the 7th Int. Conf. on Information Technology and Applications*, pp. 271–275, IEEE New South Wales (NSW) Section, Sydney, Australia (2011).
64. D. Zazula, D. Đonlagić, and S. Šprager, "Unobtrusive monitoring of biomedical signals in home environment," in *Proc. of 19th Telecommunications Forum*, pp. 31–34, Institute of Electrical and Electronics Engineers, New York (2011).
65. D. Zazula, D. Đonlagić, and S. Šprager, "Application of fiber-optic interferometry to detection of human vital signs," *J. Laser Health Acad.* **2012**(1), 27–32 (2012).
66. S. Šprager, D. Đonlagić, and D. Zazula, "Heartbeat detection applying activity index on optical interferometric signal," in *Proc. of the 11th WSEAS Int. Conf. on Instrumentation*, pp. 77–82, World Scientific and Engineering Academy and Society Press, Rovaniemi, Finland (2012).
67. D. Zazula, D. Đonlagić, and S. Šprager, "Fibre-optic interferometry as a means for the first heart sound detection," in *Advances in Applied Information Science*, M. Demiralp and A. N. Pisarchik, Eds., pp. 31–35, World Scientific and Engineering Academy and Society Press, Greece (2012).
68. S. Šprager and D. Zazula, "Optimization of heartbeat detection based on clustering and multimethod approach," in *Proc. of Annual Int. Conf. of the IEEE Engineering in Medicine and Biology Society*, pp. 5–8, Institute of Electrical and Electronics Engineers, New York, NY (2012).
69. S. Šprager, D. Đonlagić, and D. Zazula, "Overnight heartbeat monitoring by using unobtrusive optical interferometric measurements," in *Proc. of IEEE EMBS Conf. on Biomedical Engineering and Sciences*, pp. 847–852, Institute of Electrical and Electronics Engineers, New York, NY (2012).
70. S. Šprager and D. Zazula, "Heartbeat and respiration detection from optical interferometric signals by using a multimethod approach," *IEEE Trans. Biomed. Eng.* **59**(10), 2922–2929 (2012).
71. S. Šprager and D. Zazula, "Detection of heartbeat and respiration from optical interferometric signal by using wavelet transform," *Comput. Methods Programs Biomed.* **111**(1), 41–51 (2013).
72. S. Šprager and D. Zazula, "Optimization of heartbeat detection in fiber-optic unobtrusive measurements by using maximum a posteriori probability estimation," *IEEE J. Biomed. Health Inform.* **18**(4), 1161–1168 (2014).
73. A. B. Nafarrate and E. G. Rawson, "Fiber optical monitor for detecting normal breathing and heartbeat motion based on changes in speckle patterns," U.S. Patent No. 5291013 (1994).
74. J. Škrabec et al., "Preliminary detection of periodic perturbations using speckle imaging and interframe gradient," in *Recent Advances in Applied & Biomedical Informatics and Computational Engineering in Systems Applications*, M. Lazardet, Ed., pp. 251–256, World Scientific and Engineering Academy and Society Press, Florence, Italy (2011).
75. P. Podbreznik et al., "Cost-efficient speckle interferometry with plastic optical fiber for unobtrusive monitoring of human vital signs," *J. Biomed. Opt.* **18**(10), 107001 (2013).
76. F. C. Favero, J. Villatoro, and V. Pruneri, "Microstructured optical fiber interferometric breathing sensor," *J. Biomed. Opt.* **17**(3), 037006 (2012).

77. J. Mathew, Y. Semenova, and G. Farrell, "A miniature optical breathing sensor," *Biomed. Opt. Express* **3**(12), 3325–3331 (2012).
78. Q. Chen et al., "Optical fiber sensors for breathing diagnostics," *Proc. SPIE* **4616**, 14–20 (2002).
79. Y. Kang et al., "Nanostructured optical fiber sensors for breathing airflow monitoring," *Proc. SPIE* **5855**, 407–410 (2002).
80. Y. Kang et al., "Nanostructured optical fibre sensors for breathing airflow monitoring," *Meas. Sci. Technol.* **17**(5), 1207–1210 (2006).
81. M. Zyczkowski et al., "Using modalmetric fiber optic sensors to monitor the activity of the heart," *Proc. SPIE* **7894**, 789404 (2011).
82. Z. Chen, J. T. Teo, and X. Yang, "In-bed fibre optic breathing and movement sensor for non-intrusive monitoring," *Proc. SPIE* **7173**, 71730P (2009).
83. D. Lau et al., "Intensity-modulated microbend fiber optic sensor for respiratory monitoring and gating during MRI," *IEEE Trans. Biomed. Eng.* **60**(9), 2655–2662 (2013).
84. Z. Chen et al., "Simultaneous measurement of breathing rate and heart rate using a microbend multimode fiber optic sensor," *J. Biomed. Opt.* **19**(5), 057001 (2014).
85. Z. Chen et al., "Smart pillow for heart-rate monitoring using a fiber optic sensor," *Proc. SPIE* **7894**, 789402 (2011).
86. Z. Chen et al., "Portable fiber optic ballistocardiogram sensor for home use," *Proc. SPIE* **8218**, 82180X (2012).
87. C. J. Deepu et al., "A smart cushion for real-time heart rate monitoring," in *Proc. of IEEE Conf. on Biomedical Circuits and Systems*, pp. 53–56, Institute of Electrical and Electronics Engineers, New York, NY (2012).
88. Y. Zhu et al., "Ballistocardiography with fiber optic sensor in headrest position: a feasibility study and a new processing algorithm," in *Proc. of the 35th Annual Int. Conf. of the IEEE Engineering in Medicine and Biology Society*, pp. 5203–5206, Institute of Electrical and Electronics Engineers, New York, NY (2013).
89. C. Davis, A. Mazzolini, and D. Murphy, "A new fibre optic sensor for respiratory monitoring," *Australas. Phys. Eng. Sci. Med.* **20**(4), 214–219 (1997).
90. C. Davis et al., "A new sensor for monitoring chest wall motion during high-frequency oscillatory ventilation," *Med. Eng. Phys.* **21**(9), 619–623 (1999).
91. A. Babchenko et al., "Fiber optic sensor for the measurement of respiratory chest circumference changes," *J. Biomed. Opt.* **4**(2), 224–229 (1999).
92. A. T. Augousti, A. Raza, and M. Graves, "Design and characterization of a fiber-optic respiratory plethysmograph (FORP)," *Proc. SPIE* **2676**, 250–257 (1996).
93. A. T. Augousti, F.-X. Maletras, and J. Mason, "The use of a figure-of-eight coil for fibre optic respiratory plethysmography: geometrical analysis and experimental characterisation," *Opt. Fiber Technol.* **11**(4), 346–360 (2005).
94. A. T. Augousti, F.-X. Maletras, and J. Mason, "Improved fiber-optic respiratory monitoring using a figure-of-eight coil," *Physiol. Meas.* **26**(5), 585–590 (2005).
95. L. T. D'Angelo et al., "A system for respiratory motion detection using optical fibers embedded into textiles," in *Proc. of the 30th Annual Int. Conf. of the IEEE Engineering in Medicine and Biology Society*, pp. 3694–3697, Institute of Electrical and Electronics Engineers, New York, NY (2008).
96. A. Grillet et al., "Optical fibre sensors embedded into medical textiles for monitoring of respiratory movements in MRI environment," *Proc. SPIE* **6619**, 66191R (2007).
97. A. Grillet et al., "Optical fiber sensors embedded into medical textiles for healthcare monitoring," *IEEE Sens. J.* **8**(7), 1215–1222 (2008).
98. J. Witt et al., "Smart medical textiles with embedded optical fibre sensors for continuous monitoring of respiratory movements during MRI," *Proc. SPIE* **7653**, 76533B (2010).
99. J. Witt et al., "Medical textiles with embedded fiber-optic sensors for monitoring of respiratory movement," *IEEE Sens. J.* **12**(1), 246–254 (2012).
100. K. Krebber, S. Liehr, and J. Witt, "Smart technical textiles based on fiber-optic sensors," *Proc. SPIE* **8421**, 84212A (2012).
101. K. Krebber, "Smart technical textiles based on fiber optic sensors," in *Current Developments in Optical Fiber Technology*, S. W. Harun and H. Arof, Eds., pp. 319–344, InTech, Rijeka, Croatia (2013).
102. J. De Jonckheere et al., "Optical fibre sensors embedded into technical textile for a continuous monitoring of patients under magnetic resonance imaging," in *Proc. of the 30th Annual Int. Conf. of the IEEE Engineering in Medicine and Biology Society*, pp. 5266–5269, Institute of Electrical and Electronics Engineers, New York, NY (2008).
103. J. De Jonckheere et al., "OFSETH: smart medical textile for continuous monitoring of respiratory motions under magnetic resonance imaging," in *Proc. of the 31st Annual Int. Conf. of the IEEE Engineering in Medicine and Biology Society*, pp. 1473–1476, Institute of Electrical and Electronics Engineers, New York, NY (2009).
104. F. Narbonneau et al., "OFSETH: optical technologies embedded in smart medical textile for continuous monitoring of respiratory motions under magnetic resonance imaging," *Proc. SPIE* **7715**, 77151D (2010).
105. J. De Jonckheere et al., "OFSETH: a breathing motions monitoring system for patients under MRI," in *Proc. of the 32nd Annual Int. Conf. of the IEEE Engineering in Medicine and Biology Society*, pp. 1016–1019, Institute of Electrical and Electronics Engineers, New York, NY (2010).
106. J. Witt et al., "Fiber optic heart rate sensor for integration into personal protective equipment," in *Proc. of IEEE Int. Workshop on BioPhotonics*, pp. 1–3, Institute of Electrical and Electronics Engineers, New York, NY (2011).
107. M. Krehel et al., "Optical fibre based sensor for respiratory monitoring," *Sensors* **14**(7), 13088–13101 (2014).
108. M. Nishyama, M. Miyamoto, and K. Watanabe, "Respiration and body movement analysis during sleep in bed using hetero-core fiber optic pressure sensors without constraint to human activity," *J. Biomed. Opt.* **16**(1), 017002 (2011).
109. W. J. Yoo et al., "Development of respiration sensors using plastic optical fiber for respiratory monitoring inside MRI system," *J. Opt. Soc. Korea* **14**(3), 235–239 (2010).
110. W. J. Yoo et al., "Development of optical fiber-based respiration sensor for noninvasive respiratory monitoring," *Opt. Rev.* **18**(1), 132–138 (2011).
111. L. Mohanty and K. S. C. Kuang, "A breathing rate sensor with plastic optical fiber," *Appl. Phys. Lett.* **97**(7), 073703 (2010).
112. S. Muto, H. Sato, and T. Hosaka, "Optical humidity sensor using fluorescent plastic fiber and its application to breathing-condition monitor," *Jpn. J. Appl. Phys.* **33**(Part 1, No. 10), 6060–6064 (1994).
113. M. Morisawa and S. Muto, "A novel breathing condition sensor using plastic optical fiber," in *Proc. of IEEE Sensors*, pp. 1277–1280, Institute of Electrical and Electronics Engineers, New York, NY (2004).
114. K. Krebber et al., "Smart technical textiles with integrated POF sensors," *Proc. SPIE* **6933**, 69330V (2008).
115. G. Wehrle et al., "A fiber optic Bragg grating strain sensor for monitoring ventilatory movements," *Meas. Sci. Technol.* **12**(7), 805–809 (2001).
116. A. F. Silva et al., "Simultaneous cardiac and respiratory frequency measurement based on a single fiber Bragg grating sensor," *Meas. Sci. Technol.* **22**(7), 075801 (2011).
117. J. P. Carmo et al., "Application of fiber Bragg gratings to wearable garments," *IEEE Sens. J.* **12**(1), 261–266 (2012).
118. C. Zhang et al., "Smart textile sensing system for human respiration monitoring based on fiber Bragg grating," *Proc. SPIE* **7381**, 738104 (2009).
119. J. Wo et al., "Noninvasive respiration movement sensor based on distributed Bragg reflector fiber laser with beat frequency interrogation," *J. Biomed. Opt.* **19**(1), 017003 (2014).
120. J. De Jonckheere et al., "OFSETH: optical fibre embedded into technical textile for healthcare, an efficient way to monitor patient under magnetic resonance imaging," in *Proc. of the 29th Annual Int. Conf. of the IEEE Engineering in Medicine and Biology Society*, pp. 3950–3953, Institute of Electrical and Electronics Engineers, New York, NY (2007).
121. J. De Jonckheere et al., "FBG-based smart textiles for continuous monitoring of respiratory movements for healthcare applications," in *Proc. of the 12th IEEE Int. Conf. on e-Health Networking Applications and Services*, pp. 277–282, Institute of Electrical and Electronics Engineers, New York, NY (2010).

122. T. Allsop et al., "Respiratory function monitoring using a real-time three-dimensional fiber-optic shaping sensing scheme based upon fiber Bragg gratings," *J. Biomed. Opt.* **17**(11), 117001 (2012).
123. J. Hao et al., "FBG-based smart bed system for healthcare applications," *Front. Optoelectron. China* **3**(1), 78–83 (2010).
124. D. Gurkan, D. Starodubov, and X. Yuan, "Monitoring of the heartbeat sounds using an optical fiber Bragg grating sensor," in *Proc. of IEEE Sensors*, pp. 306–309, Institute of Electrical and Electronics Engineers, New York, NY (2005).
125. D. Tosi, M. Olivero, and G. Perrone, "Low-cost fiber Bragg grating vibroacoustic sensor for voice and heartbeat detection," *Appl. Opt.* **47**(28), 5123–5129 (2008).
126. T. Allsop et al., "The application of a long period grating array for respiratory function monitoring," in *Proc. of Conf. on Lasers and Electro-Optics Europe*, p. 508, Institute of Electrical and Electronics Engineers, New York (2003).
127. T. Allsop et al., "Embedded progressive-three-layered fiber long-period gratings for respiratory monitoring," *J. Biomed. Opt.* **8**(3), 552–558 (2003).
128. T. Allsop et al., "Application of long-period grating sensors to respiratory function monitoring," *Proc. SPIE* **5588**, 148–156 (2004).
129. T. Allsop et al., "Respiratory monitoring using fibre long period grating sensors," *Proc. SPIE* **5864**, 58640Q (2005).
130. T. Allsop et al., "The application of a long period grating sensors to human respiratory plethysmography," *Proc. SPIE* **6631**, 66311G (2007).
131. T. Allsop et al., "Application of long-period-grating sensors to respiratory plethysmography," *J. Biomed. Opt.* **12**(6), 064003 (2007).
132. M. D. Petrović et al., "Non-invasive respiratory monitoring using long-period fiber grating sensors," *Biomed. Opt. Express* **5**(4), 1136–1144 (2014).
133. T. Allsop et al., "Cardiac-induced localized thoracic motion detected by a fiber optic sensing scheme," *J. Biomed. Opt.* **19**(11), 117006 (2014)
134. Ł. Dziuda et al., "The device for measuring vital signs," Patent No. 217840 , Patent Office of the Republic of Poland (2010).
135. Ł. Dziuda et al., "Fiber-optic sensor for monitoring respiration and cardiac activities," *Polski Przegląd Medycyny i Psychologii Lotniczej* **17**(3), 267–284 (2011).
136. L. Dziuda et al., "Fiber-optic sensor for monitoring respiration and cardiac activity," in *Proc. of IEEE Sensors*, pp. 413–416, Institute of Electrical and Electronics Engineers, New York, NY (2011).
137. Ł. Dziuda and J. Lewandowski, "Fiber Bragg grating-based sensor for monitoring respiration and cardiac activity," in *Non-Contact Methods for Monitoring Psychophysiological Activity: Selected Papers*, Ł. Dziuda, F. Skibniewski, and W. Torbicz, Eds., pp. 7–43, Akademicka Oficyna Wydawnicza EXIT, Warszawa, Poland (2011).
138. Ł. Dziuda et al., "Fiber Bragg grating-based sensor for monitoring respiration and cardiac activity," *Elektronika: Konstrukcje, Technologie, Zastosowania* **52**(8), 98–106 (2011).
139. L. Dziuda et al., "Monitoring respiration and cardiac activity using fiber Bragg grating-based sensor," *IEEE Trans. Biomed. Eng.* **59**(7), 1934–1942 (2012).
140. Ł. Dziuda and F. W. Skibniewski, "A new approach to ballistocardiographic measurements using fiber Bragg grating-based sensors," *Biocybern. Biomed. Eng.* **34**(2), 101–116 (2014).
141. J. Lewandowski, Ł. Dziuda, and K. Celiński-Spodar, "Mechano-acoustic sensor of the cardiovascular system activity," *Elektronika: Konstrukcje, Technologie, Zastosowania* **53**(1), 77–80 (2012).
142. Ł. Dziuda et al., "Fiber-optic sensor for breathing and heart rate to be applied in the MRI environment," *Przegląd Elektrotechniczny* **88**(10b), 120–125 (2012).
143. L. Dziuda et al., "Fiber-optic sensor for respiration and heart rate monitoring in the MRI environment," *Procedia Eng.* **47C**, 1291–1294 (2012).
144. Ł. Dziuda et al., "Fiber Bragg grating-based sensor for monitoring respiration and heart activity during magnetic resonance imaging examinations," *J. Biomed. Opt.* **18**(5), 057006 (2013).
145. Ł. Dziuda, M. Krej, and F. W. Skibniewski, "Fiber Bragg grating strain sensor incorporated to monitor patient vital signs during MRI," *IEEE Sens. J.* **13**(12), 4986–4991 (2013).
146. Y.-J. Rao, "Recent progress in in-fiber Bragg grating sensors: applications," *Proc. SPIE* **3555**, 429–441 (1998).
147. G. Brady et al., "Simultaneous interrogation of interferometric and Bragg grating sensors," *Opt. Lett.* **20**(11), 1340–1342 (1995).
148. M. Majumder et al., "Fibre Bragg gratings in structural health monitoring—present status and applications," *Sens. Actuators A: Phys.* **147**(1), 150–164 (2008).
149. F. Surre, T. Sun, and K. T. Grattan, "Fiber optic strain monitoring for long-term evaluation of a concrete footbridge under extended test conditions," *IEEE Sens. J.* **13**(3), 1036–1043 (2013).
150. V. Kumar, B. C. Choudhary, and U. K. Tiwari, "FBG temperature sensor for avionics display system," *Adv. Aerosp. Sci. Appl.* **3**(1), 1–11 (2013).
151. L. Dziuda et al., "Hybrid fiber optic voltage sensor for remote monitoring of electrical submersible pump motors," *Opt. Eng.* **44**(6), 064401 (2005).
152. L. Dziuda et al., "Laboratory evaluation of the hybrid fiber-optic current sensor," *Sens. Actuators A: Phys.* **136**(1), 184–190 (2007).
153. R. C. S. B. Allil et al., "Application of fiber Bragg grating sensors in power industry," in *Current Trends in Short- and Long-Period Fiber Gratings*, C. Cuadrado-Laborde, Ed., pp. 133–166, InTech, Rijeka, Croatia (2013).
154. Y. J. Rao et al., "Optical in-fiber Bragg grating sensor systems for medical applications," *J. Biomed. Opt.* **3**(1), 38–44 (1998).
155. M. Matin, N. Hussain, and R. Shoureshi, "Fiber Bragg sensor for smart bed sheet," *Proc. SPIE* **5907**, 590706 (2005).
156. H. Xia et al., "Fiberoptic patient health multi-parameter monitoring devices and system," U.S. Patent No. 8009946 (2011).
157. S. C. Ho et al., "FBG sensor for contact level monitoring and prediction of perforation in cardiac ablation," *Sensors* **12**(1), 1002–1013 (2012).
158. E. Al-Fakih, N. A. Abu Osman, and F. R. Mahamd Adikan, "The use of fiber Bragg grating sensors in biomechanics and rehabilitation applications: the state-of-the-art and ongoing research topics," *Sensors* **12**(10), 12890–12926 (2012).
159. Y. Yu et al., "Fiber Bragg grating sensor for simultaneous measurement of displacement and temperature," *Opt. Lett.* **25**(16), 1141–1143 (2000).
160. S. Abad et al., "Fiber Bragg grating-based self referencing technique for wavelength-multiplexed intensity sensors," *Opt. Lett.* **27**(4), 222–224 (2002).
161. P. Orr and P. Niewczas, "A robust, multiplexable fiber sensor for simultaneous measurement of bend and strain," *IEEE Sens. J.* **11**(2), 341–342 (2011).
162. P. Niewczas et al., "Design and evaluation of a preprototype hybrid fiber-optic voltage sensor for a remotely interrogated condition monitoring system," *IEEE Trans. Instrum. Meas.* **54**(4), 1560–1564 (2005).
163. A. Rauf et al., "Bend measurement using an etched fiber incorporating a fiber Bragg grating," *Opt. Lett.* **38**(2), 214–216 (2013).
164. Y.-J. Rao, "In-fiber Bragg grating sensors," *Meas. Sci. Technol.* **8**(4), 355–375 (1997).
165. R. A. Betts et al., "Nonlinear refractive index in erbium doped optical fiber: theory and experiment," *IEEE J. Quantum Electron.* **27**(4), 908–913 (1991).
166. R. Kashyap, *Fiber Bragg Gratings*, Academic Press, San Diego, CA (1999).
167. A. M. Abdi et al., "Modeling, design, fabrication, and testing of a fiber Bragg grating strain sensor array" *Appl. Opt.* **46**(14), 2563–2574 (2007).
168. Ł. Dziuda, "Novel approaches to hybrid voltage and current sensing for condition monitoring of remotely operated electrical plant," PhD Dissertation, Dept. Elect. Electric. Engineering, Univ. of Strathclyde, Glasgow, UK (2007).
169. M. G. Xu, "The measurement of physical fields using optical fibers and fiber gratings," PhD Dissertation, Dept. Electron, Comput. Sci., Univ. Southampton, Hampshire, UK (1995).
170. S. M. Melle, K. Liu, and R. M. Measures, "Practical fiber-optic Bragg grating strain gauge system," *Appl. Opt.* **32**(19), 3601–3609 (1993).
171. B. T. Meggitt et al., "A novel digital phase tracking algorithm for a high resolution fibre Bragg grating based sensor system," *J. Phys.: Conf. Ser.* **15**, 74–82 (2005).

172. Q. Chen and P. Lu, "Fiber Bragg gratings and their applications as temperature and humidity sensors," in *Atomic, Molecular, and Optical Physics: New Research*, L. T. Chen, Ed., pp. 235–260, Nova Science Publishers, Inc., Hauppauge, New York, NY (2008).
173. A. Rahman et al., "Anomalous thermal dynamics of Bragg gratings inscribed in germanosilicate optical fiber," *J. Optoelectron. Adv. Mater.* **3**(1), 17–23 (2009).
174. J. Mandal et al., "Bragg grating-based fiber-optic laser probe for temperature sensing," *IEEE Photon. Technol. Lett.* **16**(1), 218–220 (2004).
175. K. T. Kim et al., "A temperature-insensitive cladding-etched fiber Bragg grating using a liquid mixture with a negative thermo-optic coefficient," *Sensors* **12**(6), 7886–7892 (2012).
176. R. González-Landaeta, O. Casas, and R. Pallàs-Areny, "Heart rate detection from an electronic weighing scale," *Physiol. Meas.* **29**(8), 979–988 (2008).
177. O. T. Inan et al., "Robust ballistocardiogram acquisition for home monitoring," *Physiol. Meas.* **30**(2), 169–185 (2009).
178. Micron Optics, Inc., "Optical sensing interrogator sm130," *Micron Optics Technical Information*, 2010, http://www.micronoptics.com/ (28 December 2014).
179. Y. B. Lin et al., "Packaging methods of fiber-Bragg grating sensors in civil structure applications," *IEEE Sens. J.* **5**(3), 419–424 (2005).
180. Y. Kim et al., "Evaluation of unconstrained monitoring technology used in the smart bed for u-Health environment," *Telemed. J. E Health* **17**(6), 435–441 (2011).
181. Philips Healthcare, "Philips magnetic resonance Achieva 1.5 T A-series," *Philips Technical Information*, 2008, http://www.healthcare.philips.com/main/ (28 December 2014).
182. Invivo International, "Precess (model 3160) MRI patient monitoring system," *Invivo Technical Information*, 2010, http://www.invivocorp.com/ (28 December 2014).
183. Ibsen Photonics A/S, "I-MON 256 and 512 USB: product specification," Ibsen Photonics Technical Information, 2013, http://www.ibsenphotonics.com/ (28 December 2014).
184. Smart Fibres Ltd, "SmartScan interrogator for fibre Bragg grating sensors," *Smart Fibres Technical Information*, 2014, http://www.smartfibres.com/ (28 December 2014).
185. M. D. Todd, G. A. Johnson, and C. C. Chang, "Passive light intensity-independent interferometric method for fibre Bragg grating interrogation," *Electron. Lett.* **35**(22), 1970–1971 (1999).
186. P. Orr and P. Niewczas, "High-speed, solid-state, interferometric interrogator and multiplexer for fiber Bragg grating sensors," *J. Lightwave Technol.* **29**(22), 3387–3392 (2011).
187. P. Orr et al., "Solid state interferometric interrogator and multiplexer for high-speed dynamic and absolute FBG wavelength measurement," *Proc. SPIE* **8794**, 87493X (2013).
188. J. M. Bland and D. G. Altman, "Statistical methods for assessing agreement between two methods of clinical measurement," *Lancet* **327**(8476), 307–310 (1986).
189. J. M. Bland and D. G. Altman, "Measuring agreement in method comparison studies," *Stat. Methods Med. Res.* **8**(2), 135–160 (1999).
190. F. D. McGlynn et al., "Component fears of claustrophobia associated with mock magnetic resonance imaging," *J. Anxiety Disord.* **21**(3), 367–380 (2007).
191. J. Enders et al., "Reduction of claustrophobia with short bore versus open magnetic resonance imaging: a randomized controlled trial," *PLoS One* **6**(8), e23494 (2011).
192. J. H. Shin et al., "Heart rate variability analysis using a ballistocardiogram during Valsalva manoeuvre and post exercise," *Physiol. Meas.* **32**(8), 1239–1264 (2011).
193. Philips Healthcare, "Respiratory motion management for CT," 2013, http://healthmanagement.org/uploads/Respiratory%20Motion%20Management%20for%20CT_white%20paper.pdf (28 December 2014).

Łukasz Dziuda is an associate professor at the Military Institute of Aviation Medicine in Warsaw, Poland. He received his PhD degree from the University of Strathclyde in Glasgow, United Kingdom in 2007 and his DSc degree from the Nałęcz Institute of Biocybernetics and Biomedical Engineering of the Polish Academy of Sciences in Warsaw in 2014. He has published nearly 40 papers on the advancement of optical sensing techniques in the fields of biomedical and power engineering.